ARL-TR-9682 • MAY 2023

Atmospheric Intelligence for Hybrid Power Advancements: Volume 2 (Whole Sky Image Percent Cloud and Sun Analyses)

by Gail Vaucher, Hailey Goodman, Brian Wang, and Michael Lee

NOTICES

Disclaimers

The findings in this report are not to be construed as an official Department of the Army position unless so designated by other authorized documents.

Citation of manufacturer's or trade names does not constitute an official endorsement or approval of the use thereof.

Destroy this report when it is no longer needed. Do not return it to the originator.

ARL-TR-9682 ● MAY 2023

Atmospheric Intelligence for Hybrid Power Advancements: Volume 2 (Whole Sky Image Percent Cloud and Sun Analyses)

Gail Vaucher and Michael Lee
DEVCOM Army Research Laboratory

Hailey Goodman
University of Central Florida

Brian Wang
Boston College (Northeastern University)

REPORT DOCUMENTATION PAGE

1. REPORT DATE	2. REPORT TYPE	3. DATES COVERED	
		START DATE	END DATE
May 2023	Technical Report	1 July 2022	30 December 2022

4. TITLE AND SUBTITLE
Atmospheric Intelligence for Hybrid Power Advancements: Volume 2 (Whole Sky Image Percent Cloud and Sun Analyses)

5a. CONTRACT NUMBER	5b. GRANT NUMBER	5c. PROGRAM ELEMENT NUMBER
5d. PROJECT NUMBER	**5e. TASK NUMBER**	**5f. WORK UNIT NUMBER**

6. AUTHOR(S)
Gail Vaucher, Hailey Goodman, Brian Wang, and Michael Lee

7. PERFORMING ORGANIZATION NAME(S) AND ADDRESS(ES)
DEVCOM Army Research Laboratory
ATTN: FCDD-RLA-ID
White Sands Missile Range, NM 88002

8. PERFORMING ORGANIZATION REPORT NUMBER
ARL-TR-9682

9. SPONSORING/MONITORING AGENCY NAME(S) AND ADDRESS(ES)	10. SPONSOR/MONITOR'S ACRONYM(S)	11. SPONSOR/MONITOR'S REPORT NUMBER(S)

12. DISTRIBUTION/AVAILABILITY STATEMENT
Approved for public release: distribution unlimited.

13. SUPPLEMENTARY NOTES
ORCID ID: Michael Lee, 0000-0002-0419-6069

14. ABSTRACT
Tactical and civilian environments depend heavily upon consistent and reliable electrical power. Solar fuel gleaned from photovoltaic (PV) technologies hold potential as a hybridized power resource. To determine the PV power contribution, knowledge of solar radiation is required. Clouds are major inhibitors of solar radiation. Whole Sky Imagers map clouds and other filters of irradiance as the radiation traverses from space onto a PV panel. Analyzing and quantifying clouds from a whole sky image was the research's goal. The method used included image analysis preparation (non-cloud feature extraction), isolating clouds, and percent cloud calculation. In the course of isolating clouds, a strong link was found that matched the sun-corona footprint with sky type, cloud layers, and cloud types. Red, green, blue thresholding was the primary approach for isolating both sun-corona and clouds, from blue sky. Multiple analysis functions were explored to see if they could improve the detailing. A sample of eight image analysis functions are described in the report, along with a summary of their usefulness to the cloud cover algorithm development. The research conducted has contributed to the hybridized power integration by further bridging the gap between the whole sky image analysis and PV power prediction.

15. SUBJECT TERMS
hybridize power, photovoltaic power, solar radiation, Whole Sky Imager, whole sky images, image analysis, percent cloud cover, percent sun disc, Military Information Sciences

16. SECURITY CLASSIFICATION OF:			17. LIMITATION OF ABSTRACT	18. NUMBER OF PAGES
a. REPORT	b. ABSTRACT	C. THIS PAGE		
UNCLASSIFIED	UNCLASSIFIED	UNCLASSIFIED	UU	82

19a. NAME OF RESPONSIBLE PERSON	19b. PHONE NUMBER *(Include area code)*
Gail Vaucher	(575) 678-3237

STANDARD FORM 298 (REV. 5/2020)
Prescribed by ANSI Std. Z39.18

Contents

List of Figures vi

List of Tables vii

Acknowledgments viii

Executive Summary ix

1. Introduction 1

1.1 Research Problem 1

1.2 Foundational Image Compression Study 2

1.3 Data Resources 3

1.3.1 WSI Image Data for Cloud Assessment Algorithm Development 3

1.3.2 WSI Image Data for Image Analysis Function Experimentation 4

1.4 Sky Assessment Techniques 5

1.5 Cloud Classification 6

1.6 Photography and Image Analysis 8

1.6.1 Lens Distortion and Artifacts 8

1.6.2 Optical Artifacts as a Function of Time and Sky Type 9

1.7 Red, Green, and Blue Thresholding 12

2. Method 12

2.1 Image Analysis Preparation: Non-cloud Feature Extraction 13

2.1.1 Determining the Sun Disc Footprint 13

2.1.2 Sun Disc Footprint Algorithm 15

2.2 Cloud Cover Determination 16

2.3 Percent Cloud Cover Algorithm 16

3. Percent Sun-Corona Disc Sky Type Correlation 16

3.1 Preliminary Sun – Sky – Cloud Type Correlation 17

3.2 Analysis of Sun – Sky – Cloud Type Correlation 18
3.2.1 CLR Sky Percent Solar Disc Analyses 19
3.2.2 OVC Sky Percent Solar Disc Analyses 20
3.2.3 PC Sky Percent Solar Disc Analyses 21

4. Alternative Image Analysis Tools 25
4.1 Gamma Correction 25
4.2 Contrast Limited Adaptive Histogram Equalization (CLAHE) 26
4.3 Image Sharpening 27
4.4 Morphological Opening 28
4.5 Morphological Erosion 29
4.6 Edge Detection 30
4.7 Inpainting 31
4.8 Circle Detection 32
4.9 Alternative Image Analysis Tools Summary 33

5. Discussion: Cloud Characterization 33
5.1 Gamma Correction and RGB Thresholding on OVC Images 34
5.2 Cloud Layer Detection 35

6. Summary and Conclusions 36

7. Recommendations 39

8. References 40

Appendix A. WSI Image Examples by Sky Type (15) and Special Cases (2) 42

Appendix B. Percent Sun Disc Algorithm Tutorial 48

Appendix C. Total Sky Function (Step 1) 55

Appendix D. Total Sun-Corona Function (Step 2) 59

Appendix E. Percent Sun-Corona Function (Step 3) **62**

Appendix F. Percent Cloud Cover Function (Step 4) **64**

Appendix G. Image Analyses Tools: Medical Applications **66**

List of Symbols, Abbreviations, and Acronyms **68**

Distribution List **70**

List of Figures

Fig. 1 WSI image examples of CLR, PC, and OVC sky types 3
Fig. 2 Lens artifacts (lens scratches, flares, wildlife deposits, and raindrops) 9
Fig. 3 CLR sky optical reflections and lens flare. Arrow shows effect direction. 10
Fig. 4 CLR sky solar disc at 1000, 1200, and 1600 MDT on 2021 September 21..... 14
Fig. 5 Comparing CLR 1200 MDT and 1300 MDT (solar noon) images 14
Fig. 6 Sun disc footprint for a sample of CLR, OVC, and PC conditions 17
Fig. 7 CLR sky cases: SR measurements..... 19
Fig. 8 CLR sky: percent solar disc results..... 20
Fig. 9 OVC sky cases: SR measurements 20
Fig. 10 OVC sky: percent solar disc results 21
Fig. 11 PC sky cases: SR measurements..... 22
Fig. 12 PC cases: pre-analysis; all images 22
Fig. 13 PC cases with OVC conditions removed 23
Fig. 14 PC cases with OVC and "no sun" images removed 23
Fig. 15 PC cases falling into OVC and "no sun" conditions only 24
Fig. 16 PC cases with OVC, "no sun," and sun-behind-thick-cloud conditions removed..... 24
Fig. 17 PC cases falling into OVC, "no sun," and sun-behind-thick-cloud conditions only..... 25
Fig. 18 Gamma-corrected image example (exaggerated on purpose)..... 26
Fig. 19 CLAHE example: original grayscale image and histogram 27
Fig. 20 CLAHE example: CLAHE processed image and histogram..... 27
Fig. 21 Image sharpening example 28
Fig. 22 Successful CLR morphological opening example..... 29
Fig. 23 Unsuccessful PC morphological opening example..... 29
Fig. 24 Morphological erosion example preserves cloud detail..... 30
Fig. 25 Edge detection example 31
Fig. 26 Inpainting function replaces the sun with mixed results..... 32
Fig. 27 Circle detection 33
Fig. 28 Overcast RGB thresholding with gamma correction 34
Fig. 29 Original (left) and gamma-corrected (right) image histogram 35

Fig. 30 PC RGB threshold, cloud layer results 36
Fig. A-1 Five clear sky cases: site B (2021)..... 44
Fig. A-2 Five overcast sky cases: site B (2021) 45
Fig. A-3 Five partly cloudy sky cases: site B (2021) 46
Fig. A-4 Two OVC special cases: 22° halo over site B (2021)..... 47

List of Tables

Table 1 WSI images (15) used for cloud algorithm development 4
Table 2 WSI images (10) used for image analysis functions experimentation.. 5
Table 3 Lens optical artifacts: low sunlight, morning cases 10
Table 4 Lens optical artifacts: low sunlight, evening cases 11
Table 5 Lens optical artifacts: high sunlight, mid-day cases 11
Table 6 Percent solar disc image data distribution and unfiltered results..... 18

Acknowledgments

The authors wish to thank Mr Sean D'Arcy for providing the 15 cases of simulated Whole Sky Imager data, and the Army Test and Evaluation Command's Meteorology Department for their field site support with the DEVCOM ARL research photovoltaic power testbed. Appreciation is extended to John Raby for his unswerving excellent technical review. Finally, special thanks go to the Technical Publishing Branch for its high-quality technical editing, specifically to Nancy Simini and Team Leader Jessica Schultheis.

Executive Summary

Tactical and civilian work environments depend heavily upon consistent and reliable electrical power. Ensuring the daily continuity of future electrical resources, while reducing its vulnerability, is possible through a managed integration or hybridization of multiple power resources. Solar fuel gleaned from photovoltaic (PV) technologies is one of several potential resources for supporting effective and efficient hybridized power systems. To determine the PV power contribution, knowledge of current and future solar radiation (SR) is required. Cloud cover is a major inhibitor of incoming SR. Consequently, there is a need to quantify this cloud cover. Whole Sky Imagers (WSIs) mounted near or on a PV panel map clouds and other potential SR inhibitors. Analyzing these maps and extracting the cloud percentage and types, is a core goal of this research.

The image analysis was built on an understanding of both the sky (cloud distribution, cloud layers, cloud types) and the image artifacts (lens distortions, optical effects, etc.). The method used for quantifying clouds within a whole sky image had three parts: image analysis preparation (non-cloud feature extraction), isolating clouds, and percent cloud calculation. During the image analysis preparation, it was noted that the sun's disc changed shape and size as a function of time. The smallest disc size occurred around solar noon and took the shape approximating a circle. Before and after this "mid-day" event, the sun's disc elongated (oval shaped) due to the fisheye lens through which the image was being taken.

In the course of isolating clouds, a strong link was found that matched sun-corona footprints with sky types. Building on this initial finding, a thesis was proposed: The relative size of the sun-corona footprint on a WSI image is correlated to the type of clouds shown on the image.

The proposed concept stemmed from the observation that percent sun-corona footprints for clear and overcast cases were within distinct ranges. Knowing a sky was defined as "Clear" automatically defined cloud cover as 0%. Likewise, an overcast sky could be labeled 100% cloud cover. If the footprint did not fall into either of these categories, the default was a Partly Cloudy sky.

Clear skies had no cloud types, by definition. Overcast cloud types were likely to be stratus or cumulus, leaving as the next step, the determination of whether the overcast cloud deck was thin (allowing more direct SR through) or thick (inhibiting direct SR). Partly Cloudy was not easily characterized. Again, the issue of thin and thick clouds challenged the sky interpretation, along with whether the sun's disc was hidden or free of clouds. When the sun was occulted by clouds, the sun disc

size imitated overcast conditions. A sun surrounded by blue sky took on the attributes of clear sky conditions.

The percent cloud calculation was defined as a basic ratio of cloud pixels with respect to total whole sky image pixels times 100%.

The determination of cloud pixels was executed using multiple image analysis functions. Red, green, blue (RGB) thresholding was the primary approach in isolating clouds from blue sky. Multiple image analysis functions were explored to see if they could improve the analysis detailing. RGB thresholding was the primary tool used, for both cloud and sun disc calculations. A sample of eight image analysis tools/functions are described in the report, along with a summary of their usefulness to the cloud cover algorithm development.

The research conducted has contributed to the hybridized power integration by further bridging the gap between the WSI analysis and the PV power prediction.

1. Introduction

Future Multi-Domain Operations require a reliable and resilient source of electricity. Integrating electrical power resource diversity is one strategy for achieving these goals while also decreasing tactical vulnerabilities of these isolated grids. Successful power hybridization is strengthened through the optimization of each contributing source. To ideally integrate solar fuels into a traditional isolated grid consisting of generators and batteries, decision aids rely on current and forecasted atmospheric intelligence. Such intelligence includes meteorological conditions predicted from forecast models and real-time sky imagery. The data are then used to predict current and future power production potential so that an energy management system (EMS) can better anticipate and maximize the use of the sun-generated electricity.

In this research, the acquisition of specialized atmospheric intelligence for solar power generation is the central focus. A solar radiation (SR) model utilizes this intelligence to quantify current and future SR magnitudes relevant to the EMS optimizing routines. One of the key parameters needed for the SR model is percent cloud cover. This parameter is typically gleaned from analyzing whole sky images. In the subsequent sections, the research problem, data resources, and various background materials needed to frame the core image analyses project are presented.

1.1 Research Problem

SR emitted by the sun travels through space and into the earth's atmosphere before reaching a photovoltaic (PV) surface that converts the irradiance into electricity. For details of that conversion, see *Atmospheric Intelligence for Hybrid Power Advancements (AIHPA), Vol 1* (Vaucher et al. 2023).

While traversing the atmosphere, solar energy is transmitted, absorbed, or reflected through each atmospheric layer. One of the greatest inhibitors of solar energy transmission is a cloud. Consequently, the SR model requires a quantification of cloud cover and cloud type. A common tool for witnessing cloud footprints over a site is a Whole Sky Imager (WSI). Developing an algorithm to transform the WSI image product into informative SR model input, such as percent cloud cover and cloud types, was the goal of this research.

1.2 Foundational Image Compression Study

This research is an extension of a WSI image analysis study documented in the *In-situ Atmospheric Intelligence for Hybrid Power Grids: Volume 3 (Analysis of Whole Sky Imager*) (Vaucher et al. 2021). The parent application involved machine learning models, which required a large quantity of WSI images to execute the SR model development and investigation. In support of this requirement, the *Vol 3* quest was pursued to maximize WSI image storage while still enabling the image analysis applications to be satisfied. Two image compression techniques were investigated: image resolution compression (IRC) with Portable Network Graphics (PNG) lossless compression, and image detail compression (IDC) executed with the Joint Photographic Experts Group (a.k.a. JPEG or JPG) format. For the IRC method, nine resolutions were evaluated. The IDC method compressed images to a fixed resolution, followed by detail recompression at 10 Quality Levels (QLs). The resulting image was then compared to the original image and tested.

The image compression impact was first quantified by the parameter peak signal-to-noise ratio (PSNR), using a threshold of 35 dB or greater to indicate acceptable results. The IDC (JPG) results showed more value in the accepted PSNR category, whereas the IRC (PNG) acceptable values were noted for the higher resolutions.

The processed images were subdivided into three sky conditions (Clear [CLR], Partly Cloudy [PC], and Overcast [OVC]) and evaluated as a function of file size. OVC showed the smallest file size for resolutions and QL data results. PC showed the greater file size, with CLR cases drifting between these two sky conditions.

The compressed images were then subjected to two diagnostic machine learning models: SR and percent cloud cover. The percent cloud cover model showed favorable results with its single image test case. Both IRC and IDC showed acceptable results at most resolutions and QLs, respectively. Numerically, the repeatability or precision of the IDC results (as file size increased) was notable.

Strengths and weaknesses for these methods and machine learning applications were characterized using samples of CLR, PC, and OVC WSI images. The best compression method was determined to be a function of the image's application(s).

The current study reported here branches off of the machine learning percent cloud cover model by determining a percent cloud cover (and cloud type) directly from the images.

1.3 Data Resources

The percent cloud cover algorithm development pursued two concurrent investigations. Both projects used data acquired by a simulated WSI. That is, a digital camera with a fisheye lens that photographed the sky from the horizon (on all sides) to zenith (straight overhead). The image's circular perimeter documented north-south-east-west horizons, with the zenith at the circular image's center point.

The digital camera images were stored in the JPG format. First, a sensor captured photographs in a binary format. The ensuing image was formed by tiny components known as picture elements, or pixels. JPG is a "lossy" compression format, meaning that image detail/quality are reduced along with storage size. Additional research regarding image compression formats for WSI data can be found in ARL-TR-9360 (Vaucher et al. 2021). Digital photograph compression can create distortions or anomalies in an image, known as manmade artifacts. The presence of artifacts and other optics-made aberrations can have a significant impact on image analysis and the determination of potential energy production due to the addition of extraneous information. Potential countermeasures for identifying and/or accommodating these artifacts are described in Section 4.

Two concurrent investigations applied their required WSI images distinctly. One investigation utilized the images to develop a model for identifying how much cloud cover and what cloud type were present in the image. The second investigation experimented with specialized functions that could be used to prepare the images for an automated model analysis. Data selected for the two related, but unique applications, are described next.

1.3.1 WSI Image Data for Cloud Assessment Algorithm Development

The cloud-assessment algorithm development began with sample cases of CLR, OVC, and PC sky conditions. Figure 1 shows an example for each of these sky conditions.

Fig. 1 WSI image examples of CLR, PC, and OVC sky types

Each sky type case consisted of images sampled every 15 min, between 1000 and 1600 MDT, over a single day at the same location. After trial runs showed success, these 3 single-day cases were expanded to include 5 days for each sky type. Table 1 lists the final 15 days of raw image data selected for this application; the date and time range of photographs are grouped by color-coded sky types. Reduced time periods, such as 210902, indicate an absence of images for that category. Appendix A, also organized by sky types, shows the 1300 MDT image for each day tabulated.

Table 1 WSI images (15) used for cloud algorithm development

Date (YYMMDD)	Time Range (MDT)	Sky Type (CLR, OVC, PC)
210826	1000-1600 MDT	CLR
210910	1000-1600 MDT	CLR
210914	1000-1600 MDT	CLR
210917	1000-1500 MDT	CLR
210921	1000-1600 MDT	CLR
210813	1000-1600 MDT	OVC
210814	1000-1600 MDT	OVC
210902	1200-1600 MDT	OVC
210905	1000-1600 MDT	OVC
210925	1000-1600 MDT	OVC
210812	1000-1600 MDT	PC
210821	1100-1600 MDT	PC
210927	1000-1600 MDT	PC
211001	1100-1600 MDT	PC
211006	1000-1600 MDT	PC

1.3.2 WSI Image Data for Image Analysis Function Experimentation

The image analysis function experimentation used a 10-day subset of the original WSI image data. The selected cases are listed in Table 2 and are grouped by their research purpose. Sun disc characterization began with CLR cases, then included OVC and PC cases. Cloud layering was tested on PC cases before subjecting advancements on a multilayered OVC sky.

Table 2 WSI images (10) used for image analysis functions experimentation

Date	Time (MDT)	Sky Condition	Research Purpose
210921	1000	CLR	Case 1 CLR Sun Disc Characterization
210921	1200	CLR	Case 2 CLR Sun Disc Characterization
210921	1300	CLR	Case 3 CLR Sun Disc Characterization
210921	1600	CLR	Case 4 CLR Sun Disc Characterization
210813	1000	OVC	Case 1 OVC Sun Disc Characterization
211006	1000	PC	Case 1 PC Sun Disc Characterization
210821	1100	PC	Case 1 PC Cloud Layering
211001	1300	PC	Case 2 PC Cloud Layering
210812	1330	PC	Case 3 PC Cloud Layering
210812	1000	OVC	Case 4 OVC Cloud Layering

1.4 Sky Assessment Techniques

There are various methods for acquiring and assessing sky conditions. The National Renewable Energy Laboratory's - Solar Radiation Research Laboratory has been acquiring WSI images for 20 years, using a system that includes an occulter to block the sun. An occulter is a mechanical arm that places a solid round disc where the sun would shine directly onto the image. The US Army Combat Capabilities Development Command (DEVCOM) Army Research Laboratory (ARL) simulated WSI does not have this feature. Consequently, the ARL camera system requires additional pre-exposure techniques to keep from overexposing the image and washing out important cloud edge details.

One cloud type assessment technique uses the cloud base height above the surface, or "ceiling". According to the American Meteorological Society (AMS) *Glossary of Meteorology*, sky ceiling describes the distance from the local earth surface to the lowest layer of clouds or obscuring phenomena, when it is "broken, overcast, or an obscuration is not classified as thin or partial" (Ceiling n.d.). Two different remote sensing techniques for assessing ceiling were explored: LiDAR (Light Detection and Ranging) and infrared sensing.

- LiDAR is an active remote sensor that "employs a radiation source generated by artificial means such as lasers" (Liou 1980). LiDAR determines the depth profile of its subject from light (Magurno et al. 2020). The system measures the distance using the time it takes for the light to travel between earth's surface, an elevated subject, and back. A typical LiDAR system measures elevation, canopy height, vertical forest structures, meteorological conditions, and species identification. A LiDAR Ceilometer samples from source (e.g., earth surface) to cloud base. The sensor can measure cloud height, ceiling layers, vertical visibility, and raw backscatter

profiles (Skyvue8 n.d.). Ceilometer applications include aviation and science, as they are typically found at airports, helipads, and in research field studies.

- Infrared sensing is another method for cloud sensing. Due to the non-spherical shape of ice particles within cirrus clouds, there has been significant irregularities with applying infrared sensing (Liou 1980). Both infrared sensing and ceilometer assessment techniques use lasers to determine the distances between the ground and the cloud layers. This is different from the WSI, which does not provide any numerical evidence of ceiling height, cloud cover, or visibility. Looking to the future, efforts to create a 3-D sky from sampling the same "ceiling" from three locations across the same surface are being investigated.

1.5 Cloud Classification

Identifying cloud types requires an understanding of cloud classification. Cloud classification is defined as "a scheme of distinguishing and grouping clouds according to their appearance, and, where possible, to their process of formation" (Cloud classification n.d.). While cloud formation is not the primary purpose of the research, determining cloud type is very relevant to the percent cloud cover algorithm development.

A cloud classification method created in 1803 by Luke Howard, and later adopted by the World Meteorological Organization, classifies clouds based on five main factors: genera, species, variety, supplementary features, and mother clouds (Cloud classification n.d.). The first factor, genera, describes the general cloud characteristics in terms of the form (the cloud's basic type)—cumulus, stratus, and cirrus. The second factor is the shape and structure of the cloud indicating its species. The third factor is the arrangement and transparency of the clouds, otherwise known as the variety. The fourth includes supplementary cloud features such as the arcus, and/or appendage cloud (i.e., pileus) forms. Lastly, the "mother cloud" factor includes clouds formed from an original cloud.

Cloud types can be broken into three layers within the troposphere, based on their height above the earth's surface. These three layers are known as the lower (cumulus), middle (stratus), and top (cirrus) levels. Note: While the standard stratus cloud is associated with mid-atmospheric levels, this extended flat-layered cloud can be found on all levels. In such cases, the cloud is labeled with two names, such as cirrostratus or stratocumulus.

The National Weather Service associates cloud types by their distance above-ground level (AGL) and their appearance (US Department of Commerce 2020). The following summarizes the primary cloud types for each major level within the troposphere:

Top-Level Clouds: The top-level cloud types can be classified by their height from the ground at approximately 20,000 ft and above (cirrus). The clouds at this level are found within the earth's upper troposphere where colder temperatures exist. As a result, the clouds are primarily composed of ice crystals and appear to be thin and wispy. The three main cloud types found within this layer are known as cirrus, cirrostratus, and cirrocumulus (US Department of Commerce 2020).

Middle-Level Clouds: The middle-level clouds manifest between approximately 6,500 and 20,000 ft (US Department of Commerce 2020). The clouds within this layer are known as altocumulus, altostratus, nimbostratus, and in special weather conditions, cumulus, and cumulonimbus (Cloud classification n.d.).

Altocumulus clouds can appear as rolls or round masses (Altocumulus n.d.). These clouds are primarily composed of water droplets with edges that are easily distinguished against a blue sky. Due to their elevation, the water droplets can become supercooled, and will freeze once in contact with a nuclei such as ice crystals or jet exhaust. The resulting state can make the cloud edges less distinguishable in an image.

Altostratus clouds are typically a darker sheen of blue or gray than the sky and cover the sky in a sheet or a layer (Altostratus n.d.). A significant feature is the darker color of the vapor-ladened clouds, which can prove challenging for image-processing.

If rain, snow, or ice droplets fall from a stratus deck, the mid-layer cloud title changes to "nimbostratus." The prefix "nimbo-" indicates rainfall, snow, or ice droplets. In appearance, nimbostratus clouds are gray or dark in color, and can be accompanied by lightning and thunder (Nimbostratus n.d.). This cloud type typically covers the sun and challenges the image processor, which must also interpret the precipitation reaching the photographic sensor.

Aside: An optical phenomenon associated with upper- or mid-layer stratus structures is a 22° halo. The halo is formed because of sun- or moonlight refraction from the ice crystal composition of stratus clouds (Halo of 22° n.d.). A halo was present in the WSI testbed case study images. The faded rainbow circle was interpreted as a white pixelation within the gray OVC cloud "background" (see Appendix A [Fig. A-4]).

Low-Level Clouds: The low-level clouds exist at 6500 ft and below (US Department of Commerce 2020). The primary low-level cloud types include cumulus and special stratus. Cumulus clouds are primarily moisture-dense and appear as cotton or cauliflower-like in their shape (Cumulus n.d.). These clouds form a sharp distinction from the blue sky and appear as a bright white masses. The color contrast between white/gray cloud and blue sky is significant. Two "special stratus" classifications within the lower layer include stratocumulus and nimbostratus. The latter cloud type distinguishes itself with the release of rainfall.

In summary, these cloud attributes are critical when interpreting their percent presence with respect to the whole sky and their impact on determining how much SR will reach the surface PV panel.

1.6 Photography and Image Analysis

A digital camera interprets colors differently than the human eye. The human eye can classify the correct color of an object due to perception and foreknowledge of what the object is supposed to look like. However, cameras are not "intelligent" enough to understand coloring in the same way. It can, however, adjust to a user-selected white color using a technique called, white balancing. White balancing for a digital image is a process for removing distorted color casts, so that an object that appears white to the human eye will also be white in the photograph (Image Quality Factors White Balance 2022). The remaining non-white colors in the image are adjusted/calibrated to the white balance selection. With the image colors "tuned," this could potentially improve image details needed for analysis.

Another factor of imaging and color processing is defining the visible light spectrum source. Visible light correlates to color temperature by explaining the warmth of a color based on the light source (Image Quality Factors White Balance 2022). Light sources, such as light-emitting diodes (LEDs) of 5000K, appear white in color, with all they illuminate having a white tone. This scenario is like the sun at its zenith (with light traveling through only 1 atmosphere). LED light between 2700 and 3000K has a yellow overtone, which projects yellow onto all objects it illuminates. When the sun nears the horizon, the number of atmospheres it traverses increases up to 29, which removes most of the higher frequencies (blues), leaving the longer wavelengths (yellow-orange-red). This shift in overtones can significantly impact an algorithm analyzing a WSI image via color contrasts.

1.6.1 Lens Distortion and Artifacts

Lens distortion and optical artifacts are some of the most repeatable non-cloud challenges when determining the percent cloud cover using a simulated WSI. The

dome-shaped, fisheye WSI lens creates a barrel distortion as it translates pixels onto the flat rectangular Liquid-Crystal Display (LCD) screen of the WSI/camera. This attribute has the potential for creating distortions toward the image edges. To counter this effect, an image segmentation function was used as part of the algorithm development and is described in Section 2.

Other lens artifacts observed in this study included lens scratches, lens flares, wildlife deposits, and precipitation. Figure 2 presents examples of lens scratches (left image, large red circle), lens flare (left image, small red circle), wildlife deposits (center image/red circle), and raindrops (right image). Optical reflections and lens flares are primarily a function of the sun angle and are explained in the next section.

Fig. 2 Lens artifacts (lens scratches, flares, wildlife deposits, and raindrops)

1.6.2 Optical Artifacts as a Function of Time and Sky Type

The optical artifacts generated from a dome-shaped fisheye lens change as a function of time. That is, when the sun is low in the sky, the direct sunlight passes through the fisheye lens and reflects off the opposite side of the dome lens creating nonlinear optical artifacts. As the sun rises, these secondary light bending/refracting features lower toward the image's horizon until they exit the perimeter of the image. Figure 3 demonstrates the effects of sunlight passing through the WSI dome lens, under clear skies, as a function of time. A red arrow showing the direction of these optical effects is provided in the image.

Fig. 3 CLR sky optical reflections and lens flare. Arrow shows effect direction.

To better characterize the various artifacts, the 1000–1600 local time (LT) WSI data were separated into two categories based on the sun's elevation above the horizon: (1) low morning and evening sun (first and last images of the day's sequence) and (2) a high mid-day sun (MDT). Each category was further divided into the three basic sky types: CLR, PC, and OVC. Visual artifacts in each image category were identified and labeled by the feature and its main cause (classification). Countermeasures for removing/rectifying the artifact were suggested. The results are shown in Tables 3–5.

Table 3 Lens optical artifacts: low sunlight, morning cases

Date	Time	Sky Type	Artifact	Artifact Classification	Countermeasure
210826	1000	Clear	Scratches, Lens Flare	Hardware, Optical	Morphological Opening
210910	1000	Clear	Scratches, Lens Flare	Hardware, Optical	Morphological Opening
210914	1000	Clear	Scratches	Hardware	Morphological Opening
210917	1000	Clear	Scratches, Lens Flare	Hardware, Optical	Morphological Opening
210921	1000	Clear	Scratches, Lens Flare	Hardware, Optical	Morphological Opening
210813	1000	Overcast	Raindrops	Weather	None
210814	1000	Overcast	Raindrops	Weather	None
210902	1200	Overcast	None	N/A	None
210905	1000	Overcast	None	N/A	None
210925	1000	Overcast	None	N/A	None
210812	1000	Partly Cloudy	None	N/A	None
210821	1100	Partly Cloudy	Scratches	Lens	Morphological Erosion
210927	1000	Partly Cloudy	None	N/A	None
211001	1100	Partly Cloudy	None	N/A	None
211006	1000	Partly Cloudy	Scratches, Dirty Lens	Hardware, Wildlife	Morphological Erosion, Gamma Correction

Table 4 Lens optical artifacts: low sunlight, evening cases

Date	Time	Sky Type	Artifact	Artifact Classification	Countermeasure
210826	1600	Clear	Scratches, Lens Flare	Hardware, Optical	Morphological Opening
210910	1600	Clear	Scratches, Lens Flare	Hardware, Optical	Morphological Opening
210914	1600	Clear	Scratches	Hardware	Morphological Opening
210917	1500	Clear	Scratches, Lens Flare	Hardware, Optical	Morphological Opening
210921	1600	Clear	Scratches, Lens Flare	Hardware, Optical	Morphological Opening
210813	1600	Overcast	None	N/A	None
210814	1600	Overcast	None	N/A	None
210902	1600	Overcast	None	N/A	None
210905	1600	Overcast	None	N/A	None
210925	1600	Overcast	None	N/A	None
210812	1600	Partly Cloudy	Scratches	Hardware	Morphological Erosion
210821	1600	Partly Cloudy	None	N/A	None
210927	1600	Partly Cloudy	None	N/A	None
211001	1600	Partly Cloudy	Scratches	Hardware	Morphological Erosion
211006	1600	Partly Cloudy	Dirty Lens	Wildlife	Gamma Correction

Table 5 Lens optical artifacts: high sunlight, mid-day cases

Date	Time	Sky Type	Artifact	Artifact Classification	Countermeasure
210826	1200	Clear	Scratches, Lens Flare	Hardware, Optical	Morphological Opening
210910	1200	Clear	Scratches	Hardware	Morphological Opening
210914	1200	Clear	Scratches	Hardware	Morphological Opening
210917	1200	Clear	Scratches	Hardware	Morphological Opening
210921	1200	Clear	Scratches	Hardware	Morphological Opening
210813	1200	Overcast	None	N/A	None
210814	1200	Overcast	Raindrops	Weather	None
210902	1400	Overcast	None	N/A	None
210905	1200	Overcast	None	N/A	None
210925	1200	Overcast	Raindrops	Weather	None
210812	1200	Partly Cloudy	Scratches, Lens Flare	Hardware, Optical	Morphological Erosion, Gamma Correction
210821	1200	Partly Cloudy	None	N/A	None
210927	1200	Partly Cloudy	Scratches	Hardware	Morphological Erosion
211001	1200	Partly Cloudy	None	N/A	None
211006	1200	Partly Cloudy	Scratches, Lens Flare, Dirty Lens	Hardware, Optical, Wildlife	Morphological Erosion, Gamma Correction

The greatest number of artifacts were found in the CLR sky cases. Low sunlight conditions not only distorted the solar disc but generated the most reflections. Lens scratches appeared around the sun disc, while the lens flare was found in a straight line opposite the sun. High-elevation/mid-day sunlight under CLR sky resulted in the appearance of more scratches due to the intensity of the sun and less lens flare due to the orientation onto the digital image.

OVC sky cases generally did not have artifacts, except for the appearance of raindrops.

Finally, if the sun disc was covered under a PC sky case, no artifacts were evident. Once the sun was no longer hidden, the artifact pattern followed those of CLR sky conditions.

The image processing tools investigated to correct contrast, remove artifacts, and/or refine details while preparing for the percent cloud cover calculations, are presented in Section 4.

1.7 Red, Green, and Blue Thresholding

One of the common image analysis methods is called the red, green, and blue (RGB) thresholding technique. The RGB technique splits the digital image into red, green, and blue frequency planes. The digital nature of color is presented as an 8-bit color, consequently there are 2^8 or 256 variations with each primary color. Combining these three (red, green, blue) produces colors ranging from black (0, 0, 0) through white (255, 255, 255). In between there are 16,777,216 possible colors. Through trial and error, a human analyzer can adjust the individual RGB frequencies to extract or enhance key elements or objects within the image. For this study, clouds were the primary target, so the focus was on the red frequency plane. The RGB threshold implementation will be elaborated on in the next section.

2. Method

The method used to develop percent cloud-cover and cloud-type algorithms began with the foundational background investigation, described previously. A subsequent three-step strategy followed, which included:

Step 1. Identify and extract non-cloud features from the whole sky image.

Step 2. Isolate clouds from sky.

Step 3. Calculate percent cloud cover.

The basic equation used for calculating the percent cloud cover was

$$Cloud\ Footprint = \frac{Total\ cloud\ pixels}{Total\ sky\ pixels} \times 100\% \qquad (1)$$

The numerator is the total number of pixels found within the footprint of all clouds on the sky image. The denominator is the total pixel count of the entire circular sky image (not including the black rectangular frame).

The next sections describe these steps.

2.1 Image Analysis Preparation: Non-cloud Feature Extraction

The process for determining the percent cloud cover in a whole sky image, began by addressing the known non-cloud elements. Such elements included the black frame that fills the space between the photo's rectangular edges and the circular sky. Due to the circular consistency of the sky image, the sky pixels could be extracted from the frame using a MATLAB Image Segmenter function and its circle mask.

The land features were limited to the sky circle perimeter and were consistently very dark in color with respect to the atmosphere. Using the Image Segmenter to adjust the circle mask, these land features were easily pruned so that their contribution became insignificant (see Appendix A).

Focusing on just the circular sky image, optical artifacts caused by the sun's interaction with the dome-shaped lens were determined to have a time dependency. For this phase of the algorithm development, the images studied were chosen during time intervals that minimized the optical artifact presence. (See Section 1.6)

The brightest object in each daytime photo was the sun. Normally, WSIs have an occulter device that blocks the intense brilliance of the solar disc; however, employing a standard camera with a fisheye lens, the radiant sun had to be attended to in a postprocessing algorithm. The next subsections describe the method used for identifying and addressing the solar disc in each WSI image.

2.1.1 Determining the Sun Disc Footprint

In a WSI image, the sun disc appears to have the same basic color as a cloud; therefore, the automated image analysis process considered it a cloud. To remove the solar disc data from the cloud pixel count calculation, characterizing the solar disc was required.

Most human viewers perceive the solar disc to be round. However, after examining the 2021 September 21 CLR sky case images at three different LTs (1000, 1200 and 1600 MDT), the solar disc was **not** found to be consistently round. The minimum disc size (near round) for the three selected images occurred at 1200 MDT, with the morning and evening solar discs being slightly ellipsoidal. Figure 4 shows the original image, a red threshold adjusted image (0–245) and an inverted mask image for the morning mid-day and late afternoon WSI images. The net effect is reasonable, after considering the geometry of projecting a solar disc onto the flat WSI image. The highest angle (zenith position) would present its most symmetrical shape along the sun's east to west pathway. However, the 1200 MDT sample was not found at its WSI zenith.

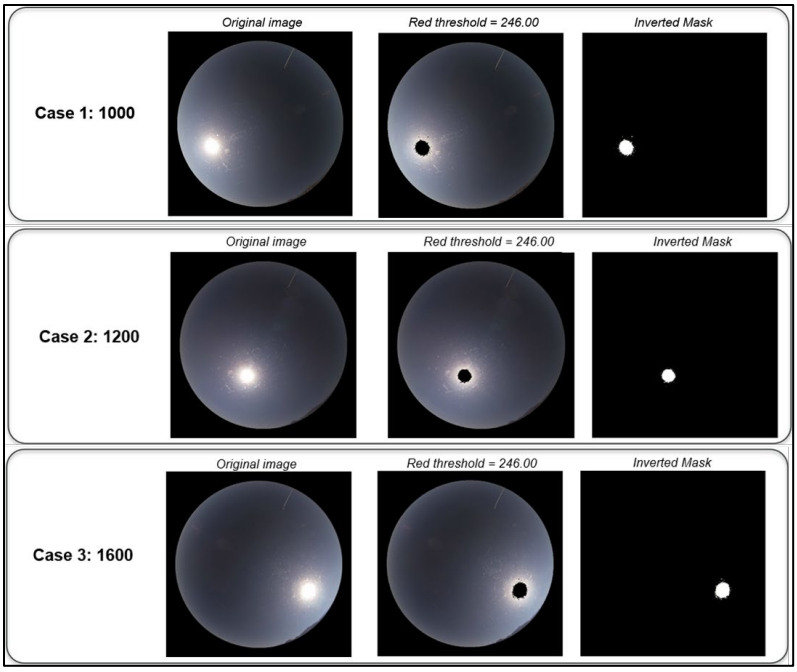

Fig. 4 CLR sky solar disc at 1000, 1200, and 1600 MDT on 2021 September 21

Before extracting the 1200 MDT WSI images for further analyses, image time stamps were tested to confirm their nearest "solar noon" (zenith) representation. The need to adjust the sampling by 1 h (Daylight Time to Standard Time) was implemented since all cases fell between March and November. Figure 5 compares the 1200 MDT and 1300 MDT (1200 MST) images under a CLR sky. The yellow lines delineate the horizontal and vertical center locations. The "solar noon" images were taken to be 1300 MDT, or 1200 MST. The difference between a true zenith and the sun's highest rise in the day (local zenith) is related to the latitude of the image sample. For Fig. 5 (Sep 21), the latitude was about 32° north.

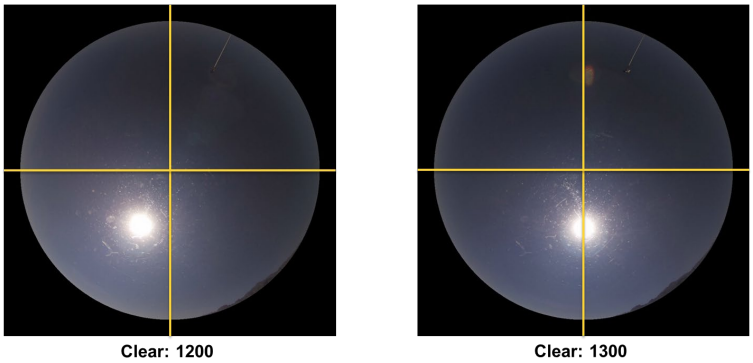

Fig. 5 Comparing CLR 1200 MDT and 1300 MDT (solar noon) images

2.1.2 Sun Disc Footprint Algorithm

Isolating and quantifying the brightest subject in the WSI image, namely the sun, was the next step in the process. A tutorial for isolating the sun disc is provided in Appendix B; individual steps are described in Appendices C through E. To quantify the solar presence, the sun's corona was included in the sun disc footprint, and Eq. 1 was modified slightly:

$$SunCorona\ Footprint = \frac{Total\ SunCorona\ pixels}{Total\ sky\ pixels} \times 100\% \qquad (2)$$

The *SunCorona Footprint* Eq. 2 totals all pixels representing the sun and its glory/corona in the numerator. Contrasting this value against the total pixels shown as "the sky," defines the percent sun disc. The process of isolating and quantifying the sun-corona pixels from the rest of the whole sky pixels utilized three MATLAB functions: the Image Segmenter, Color Thresholder, and Image Region Analyzer.

The Image Segmenter extracted the circular sky image from its black square frame. This action required the user to draw the initial circle around the sky image or region of interest (ROI), after which that footprint was turned into a binary array. That is, the ROI (the sky) was defined as 1s. The non-ROI pixels (black frame) were defined as 0s. The black frame or "dead space" size was relatively consistent between all images, enabling this action to be a repeatable task between images. Once the frame was removed (given 0 values), the ROI was masked, tallied, and used as the denominator for Eqs. 1 and 2.

Understanding that the sun is not always circular (see Section 2.1.1), the MATLAB Color Thresholder function was used. This function focused on the sun's intensity, which distinguished it from standard clouds and blue sky. To isolate the brilliant solar pixel frequency, the function's RGB thresholds were manually set. The Color Thresholder identified the sun as a frequency of red pixels with an intensity from 0–245.00 (A post-study investigation suggested the subjective value might be 225). The frequency of the pixels remained true for all test images in this study. This function then transformed the sun-mask, created by changing the RGB thresholds, into a binary array and inverted the results. The now-white pixels of the sun and its corona (1s) were tallied and this number was inserted into the numerator of Eq. 2.

The Image Region Analyzer was used to assist in independently validating the two previous function outputs. The final step in the SunCorona algorithm was to calculate the percent that the sun-corona occupied within the sky image. Using Sun-Corona Footprint equation (Eq. 2), the sun disc pixel count was divided by the total sky pixel count and multiplied by 100%. As a cross-check, the percent of non-sun disc pixel count (blue sky) should be equal to 1 minus the percent sun-corona value.

2.2 Cloud Cover Determination

To determine the cloud cover in an image, the same sun disc masking technique was used. A MATLAB color thresholder function split the digital image into red, green, and blue frequency planes. Adjusting the red frequency isolated the various cloud types and created a cloud mask. Mask pixels were tallied, the sun-corona count was subtracted as appropriate, and the final value used as the numerator in Eq. 1.

For PC images, and/or multiple layer cloud cases, two masks had to be generated. For example: A PC image with both top-layer cirrus and low-layer cumulus required manually selecting RGB thresholds for the top layer to mask the "thinner" clouds, followed by isolating a cloud mask for the "thicker" bottom layer. Masks were compared (to adjust for removing overlapping ROI), then the unique cloud pixel counts from both masks were added and sun count was removed as appropriate. The final pixel number was used as the Eq. 1 numerator.

2.3 Percent Cloud Cover Algorithm

The final step in the Percent Cloud Cover algorithm was to compare the calculated cloud pixel count with the total whole sky image pixel count. When layered clouds were observed, this ratio was expanded to include percent top-layer clouds ("thin"), percent bottom-layer clouds ("thick"), and total blue sky. Under normal conditions, these three numbers equaled 100%, which reinforced a high confidence level. Appendix F provides additional details.

3. Percent Sun-Corona Disc Sky Type Correlation

An unexpected correlation was revealed while pursuing a more in-depth characterization of the solar disc pixel count in the whole sky images. Under CLR, the round yet almost time-symmetrical distortions observed from sunrise to sunset prompted an interest in how these changes might be observed under the three basic sky conditions, namely, CLR, PC, and OVC. Selecting a sample day that presented consistent sky type conditions between 1000 and 1600 MDT (0900–1500 MST), the resulting sun-corona percentages distinguished themselves.

3.1 Preliminary Sun – Sky – Cloud Type Correlation

OVC conditions for the 2021 August 13 sample case produced percent sun-corona results that were consistently less than 0.3%. The 2021 September 21 CLR sun disc ranged between 0.35% and 0.55%. The 2021 October 6 PC conditions included most of the remaining values. Figure 6 shows all three sample sky type results for the 15-min samples taken between 1000 and 1600 MDT.

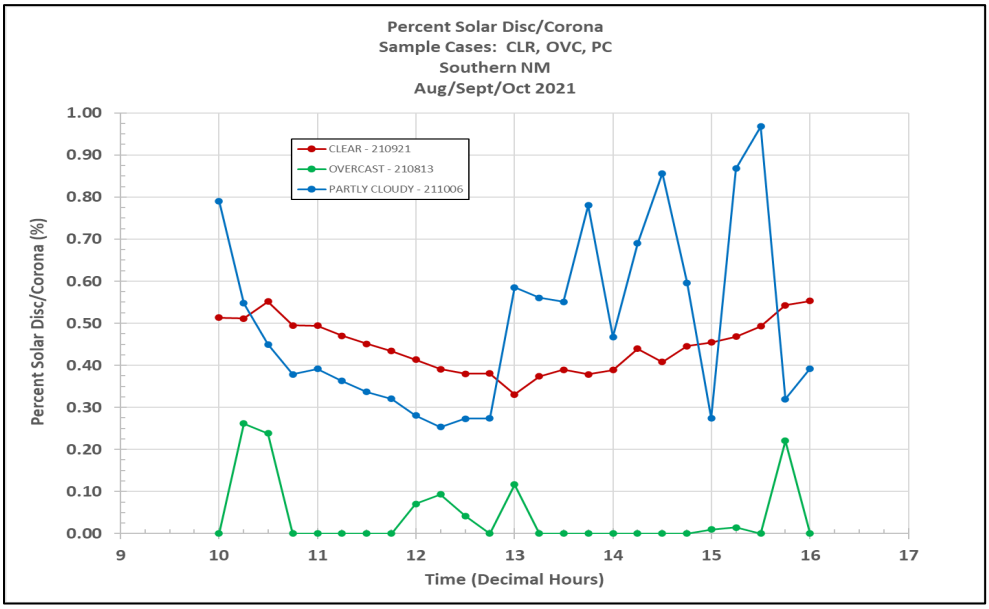

Fig. 6 Sun disc footprint for a sample of CLR, OVC, and PC conditions

Presuming these patterns are consistent beyond the sample cases, a tentative thesis was proposed: The relative size of the sun-corona footprint on a WSI image is correlated to a sky condition and therefore the type of clouds shown on an image. Pending a validated thesis, the ability to determine cloud type presents a significant benefit. For example:

- Sun disc percentages within the range of a CLR sky would indicate no clouds (radiation inhibitors) present. The output tally presented to the receiving model application would be 0% clouds/100% blue sky, and no cloud types reported on all levels (low, mid, top).
- If the sun disc percentage indicated an OVC sky, two possible subsequent OVC conditions would be considered: thin OVC and thick OVC. OVC clouds that are thin allow more SR to pass through, whereas moisture-ladened clouds filter the solar fuel, inhibiting the radiation's progress in reaching the earth's surface, resulting in reduced PV power production. Thick OVC would likely be mid- and/or low-level clouds that sustain water

droplets and reduce PV power production opportunities, whereas a thin OVC would likely be mid-layer or high-level cirrus clouds, potentially sporting cold water droplets and/or ice crystals. The higher the cloud, the colder the temperatures and the more likely the cloud material will be ice crystals (which allow more radiation to pass through them). While not pursued at the time of this study, clarifying solar intensity was considered a potential resource for the determining a thin or thick cloud status.

- If the percent sun-corona did not fall within the CLR and OVC ranges, the default sky type would be PC. This condition, and/or a mixture of cloud types pose the greatest challenge in calculating how much SR will reach the ground or PV panel mounted near the ground.

3.2 Analysis of Sun – Sky – Cloud Type Correlation

The correlation of percent sun disc with sky type was considered worthy of pursuit, based on the initial findings (Fig. 6) and the potential image analysis insights (Section 3.1). Consequently, 15 cases (5 days of CLR, OVC, and PC) with their 15-min samples/355 raw data WSI images, were selected. The 1000–1600 LT samples selected helped to reduce the potential for lens artifacts. A closer look at each day, however, revealed a need to refine the sky type labeling for each of the photographs. The net result yielded 121 CLR, 108 OVC, and 96 PC WSI images still representing 5 different days per sky type from the 2021 August through October time period. Each image selected was subjected to the same sun-corona pixel count analyses as the trial run. Table 6 captures the unfiltered processed image data distribution, along with the sun-corona pixel statistical analysis results of the investigation. The results are described by sky type in the next sections.

Table 6 Percent solar disc image data distribution and unfiltered results

Parameter	Sky Type		
	CLR	**OVC**	**PC**
Image Date (Image Count) [YYMMDD] (# of images)	210826 (25) 210910 (25) 210914 (25) 210917 (21) 210921 (25)	210813 (25) 210814 (25) 210902c (12) 210905c (22) 210925 (25)	210812 (25) 210821 (25) 210927 (25) 211001 (21) 211006 (25)
Total image count	121	108	96
Max *Percent Sun-Corona Disc*	0.5530	0.2613	1.7084
Min *Percent Sun-Corona Disc*	0.1974	0.0000	0.1019
Avg *Percent Sun-Corona Disc*	0.3350	0.0304	0.3566

3.2.1 CLR Sky Percent Solar Disc Analyses

The CLR sky images included a sun disc and between 90% to almost 100%, blue sky. The non-blue sky region (up to 10% of the image) was filled with clouds. In the cases selected, none of the clouds covered the sun. Figure 7 presents 1-min averaged SR data sampled during each of the selected CLR cases. The pink dashed lines frame the time period between which the WSI images were acquired (sampled once every 15 min). Where the time series curves are Gaussian shaped and smooth, there were no clouds covering the sun. Only on 2021 September 14, after 1500 MDT, does the SR drop, indicating the presence of cloud cover. For the analysis, the September 14 case used only images taken between 1000 and 1500 MDT, reducing the total image count from 125 to 121.

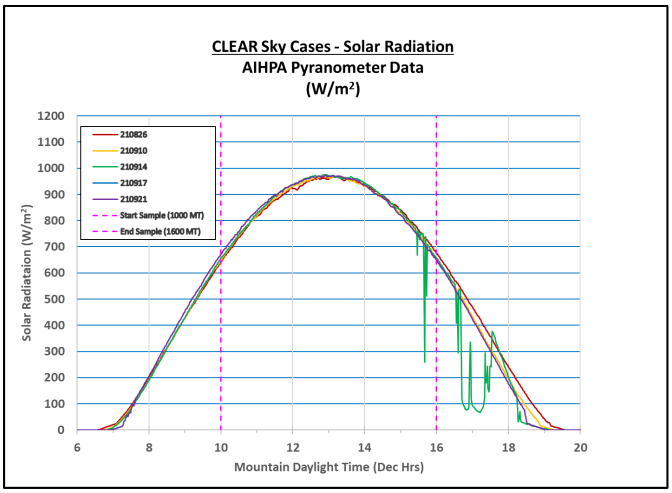

Fig. 7 CLR sky cases: SR measurements

Figure 8 shows the calculated percent sun disc range. The general pattern fell between 0.20% and 0.55%. Each day of results shows a general symmetry centered around a 1300 MDT (~ solar noon) minimum percentage. The September 21 (Autumnal Equinox) case, with the astronomically determined daily balance of sunlight and darkness, reported the widest minimum/maximum spread (about 0.2%).

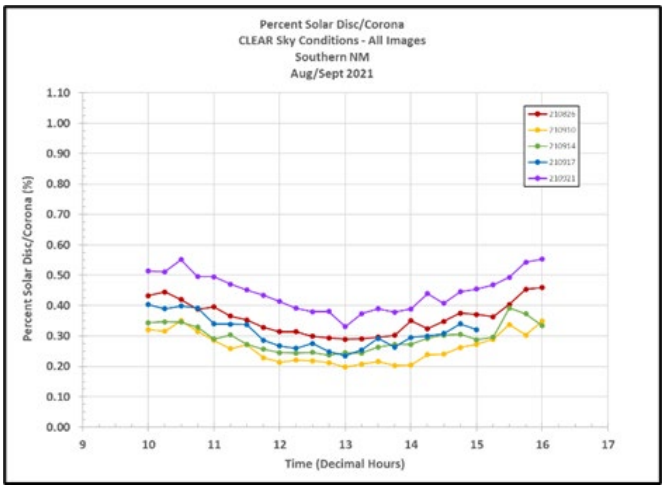

Fig. 8 CLR sky: percent solar disc results

3.2.2 OVC Sky Percent Solar Disc Analyses

The OVC case images were peppered with PC images in 2 of the 5 days (210902 and 210905). Raindrops were witnessed on images in four of the days, namely 210813, 210814, 210902, and 210905. While the raindrop images were included in the analysis, the PC images were extracted, leaving 108 OVC images.

Cross-checking the OVC days against independently sampled SR magnitudes (see Fig. 9), the bulk of the OVC conditions tended to limit their maximum values to less than 500 W/m^2. The exceptions were 210902 (green) and 210905 (blue), which were the two days that reported a mix of OVC and PC. Note: The pink lines in Fig. 9 bracket the time period of image sampling.

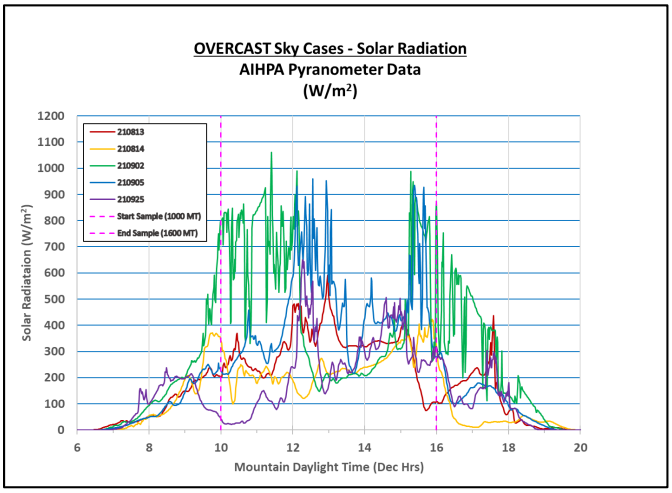

Fig. 9 OVC sky cases: SR measurements

Figure 10 shows the percent sun disc results from the net OVC images. The general pattern fell below 0.3%, with a significant portion reporting 0%. A second closer look at the source images found that the 210813 (red), 1015 and 1030 MDT images showed a discernable solar disc through "thin" OVC clouds, which explains the greater percent magnitudes for those times. The large percent results from the 230905 case (blue), seems to stem from the nearly PC conditions (9/10 cloud cover) present at 1215–1300 MDT, and 1545 MDT. A third novelty observed was a 22° halo created by "thin" OVC clouds of 230925 (purple) case. The time of these occurrences were 1215–1230 MDT and 1415–1500 MDT. The halo conditions reported an increased (nonzero) solar disc percentage; however, the values were still within "normal" OVC values.

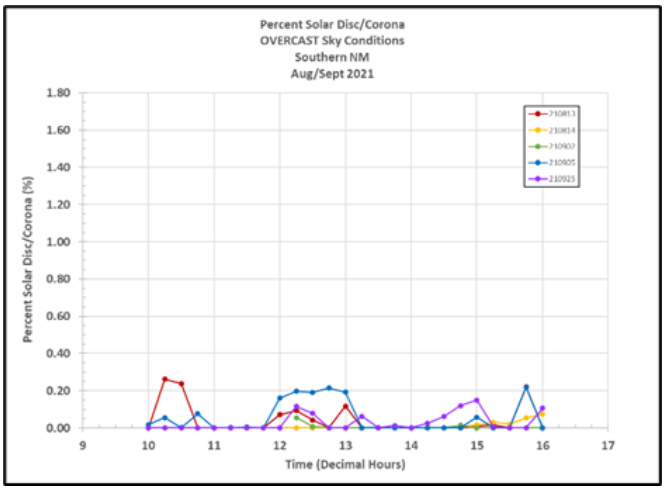

Fig. 10 OVC sky: percent solar disc results

3.2.3 PC Sky Percent Solar Disc Analyses

The PC sky case images were the most challenging to characterize. PC cases were initially defined as having clouds and blue sky present in the image. This classification attribute was later refined after reviewing the initial percent solar disc results and the SR timeseries for the 5 selected days.

Starting with PC case SR times series, Fig. 11 shows the discernable gaussian curve of the CLR cases; however, there are numerous deep, sharp drops indicating a potential mix of nearly OVC conditions within these days. There are also multiple cases where the SR magnitude seems to exceed the CLR sky values, which is a topic for another study.

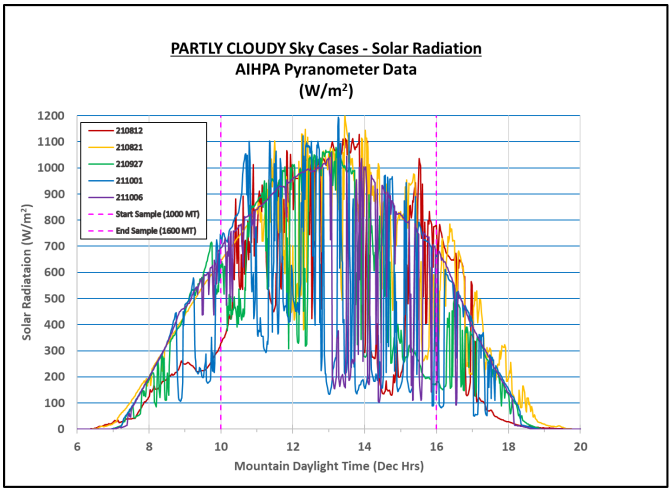

Fig. 11 PC sky cases: SR measurements

The initial, unfiltered Percent Sun-Corona results for the PC image cases are presented in Fig. 12. Returning to the raw images and redefining OVC to mean a sky with 90% or greater cloud cover, about 7% of the 15-min PC case images were evaluated as OVC, and consequently were removed. Conversely, PC conditions were now defined as being between 10% and 90% cloud cover. Figure 13 shows the Percent Sun-Corona results for PC cases with the OVC samples removed. As anticipated, with the OVC images removed, the extremely low magnitude results are absent in the updated PC percent sun plot.

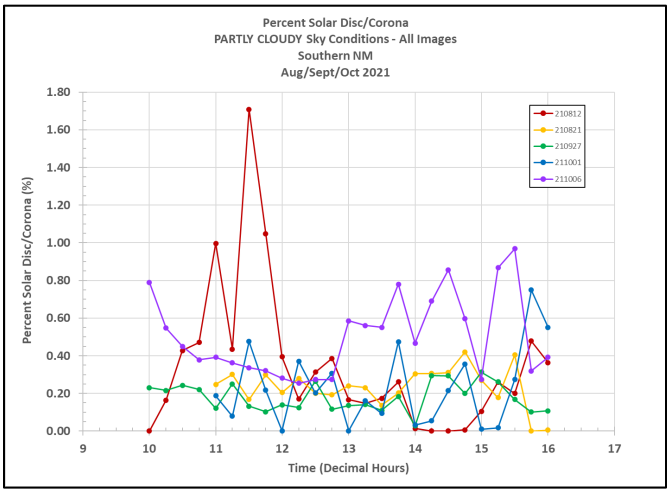

Fig. 12 PC cases: pre-analysis; all images

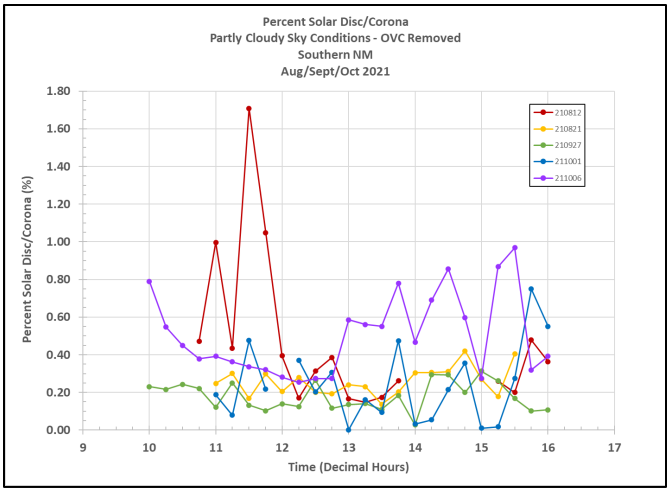

Fig. 13 PC cases with OVC conditions removed

The next PC refinement was to determine if the image had a visible sun or if the solar disc was obscured by clouds. About 12% of the initial PC images had no sun for the image analyzer to consider. Since these "no sun" cases were reporting 0% sun pixels (imitating OVC results), their conditions were noted, and those photos were extracted.

Figure 14 shows the percent sun disc calculated for PC cases that excluded OVC (sky between 9/10 and 10/10 cloud cover) and the "No Sun" images. For a balanced perspective, Fig. 15 shows the removed percent solar disc values, which are generally, less than 0.5%. The 210821, 1030 MDT image showed a 9/10 cloud cover, with the sun's glory spread out into the covering cloud deck. The 211001, 1345 MDT image had no circular sun footprint; however, the covering cloud perimeter was strongly illuminated.

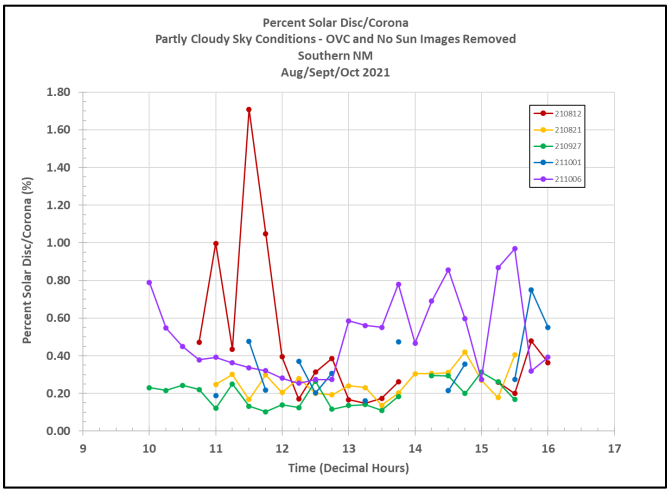

Fig. 14 PC cases with OVC and "no sun" images removed

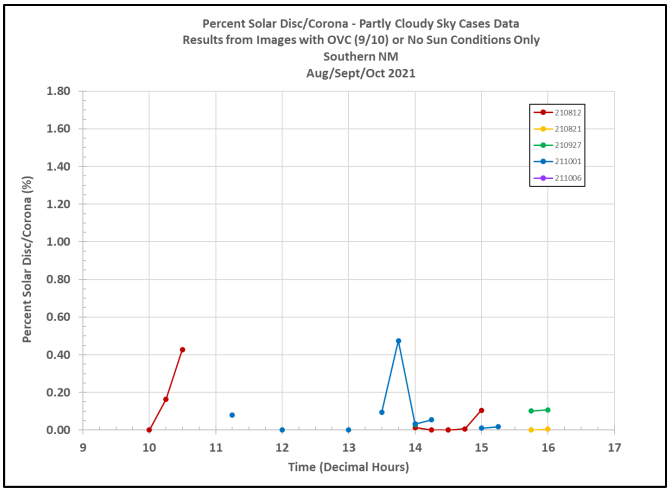

Fig. 15 PC cases falling into OVC and "no sun" conditions only

The final effect evaluated sought to discern between thin and thick cloud cover. Since thick clouds covering the sun produced magnitudes falling into the OVC category, flagging and removing these samples was the next step. Figure 16 shows the results generated when the images with a sun positioned behind thick clouds were removed. The net image count was 96 cases.

The most significant impact from this final effect was the removal of the larger percent magnitudes, bringing the final range of PC values considered, closer to a CLR sky pattern. To assist with the contrast, Fig. 17 shows the percent values of the OVC, "no sun," and sun-behind-thick cloud conditions. From a gross perspective, this latest filter primary removed the scattered outlier magnitudes. The refined PC results now ranged between about 0.1% and 0.9%. Note: When the images were removed from the evaluation, they were not reassigned to another category.

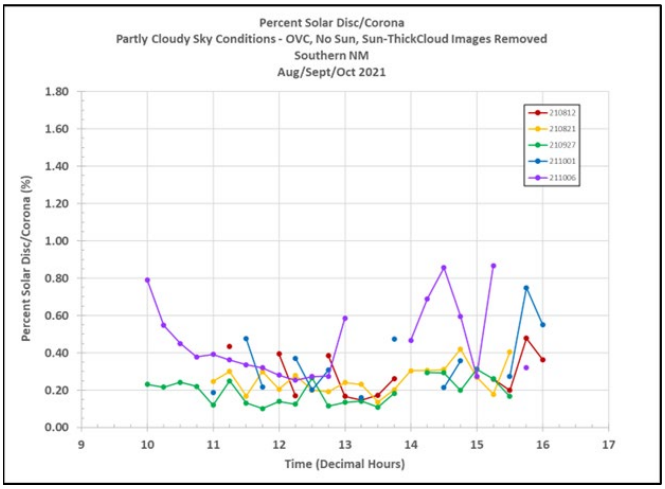

Fig. 16 PC cases with OVC, "no sun," and sun-behind-thick-cloud conditions removed

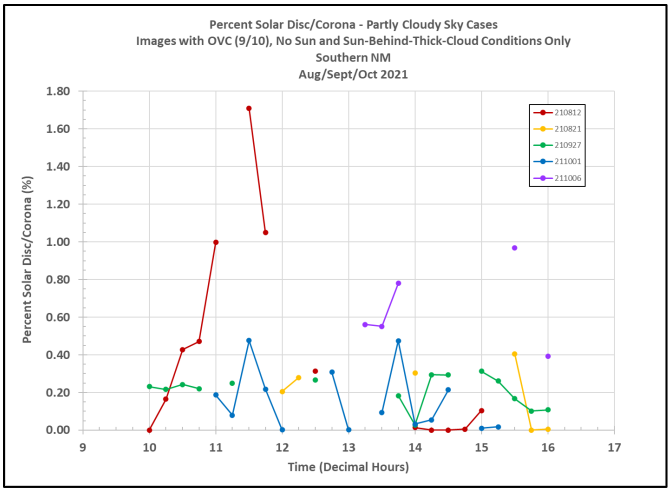

Fig. 17 PC cases falling into OVC, "no sun," and sun-behind-thick-cloud conditions only

The next section presents a summary of eight alternative image analysis tools considered for preparing the WSI images for their cloud evaluation. A demonstration of each function is provided, along with its possible application in the image analysis process.

4. Alternative Image Analysis Tools

Digital photography and image editing software have gone through significant growth over the past couple of decades. Currently, much-higher-quality photographs are being taken with greater detail and denser pixel count using relatively simple equipment and techniques. Typically, image processing utilizes graphics and photographic software to correct known mistakes, imperfections, or inaccuracies in the photo. Images can be enhanced with techniques such as sharpening, gamma correction, and contrast adjustments. These functions produce natural-looking images without introducing additional data. In this section, eight MATLAB image processing tools are reviewed. These functions were selected based on their ability to correct contrast, remove artifacts, and refine WSI image detail needed to calculate the percent cloud cover.

4.1 Gamma Correction

Gamma correction was originally used to fix the deficiencies (nonlinearity) of cathode ray tube (CRT) monitors, which commonly made their dim values darker. With the gamma correction, CRT data became overly bright so that the output would better service the computer screen's user, appearing as natural as possible (Fulton 2022). The tool was investigated in this study to correct deficiencies in image tonal data values, which decreases differences in how a camera captures

information compared to our eyes. In Fig. 18, the original image is on the left; the gamma-corrected image on the right. Here the corrected image is purposefully overcorrected to demonstrate the function of the tool. The brighter cloud areas still retain their detail while darker areas are easily identified.

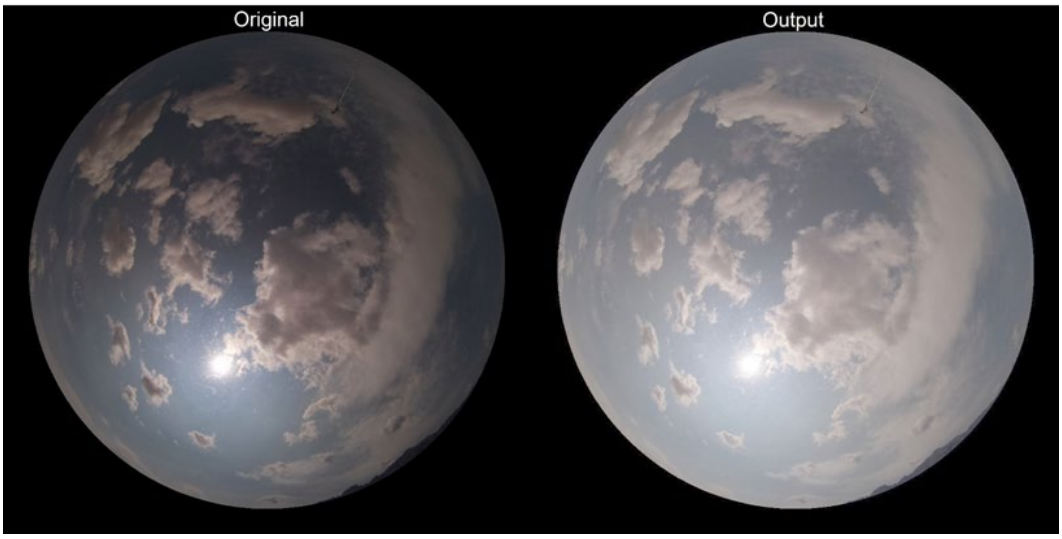

Fig. 18 Gamma-corrected image example (exaggerated on purpose)

4.2 Contrast Limited Adaptive Histogram Equalization (CLAHE)

The CLAHE is a method of contrast adjustments using an image's histogram. The histogram is a graphical representation of tonal distribution within the digital image. The most frequent intensity values are conditioned for an even distribution, thus evening out areas of lower contrast (Huamán 2022). In the CLAHE function, an image is divided into small blocks called "tiles" and equalized with contrast limiting thresholds. If a histogram bin is above a specified contrast limit, those pixels are uniformly distributed to other bins before applying equalization. Bilinear interpolation is then applied to remove artifacts in tile borders. This tool was considered for this study, based on its ability to improve image contrast that would better identify artifacts and make the sky/cloud layers more easily discernable.

Figures 19 and 20 provide an example of the CLAHE application. Figure 19 shows the original image using gray scale, along with the corresponding gray scale histogram. The subject artifact, made by the local birds, is highlighted by the red circle.

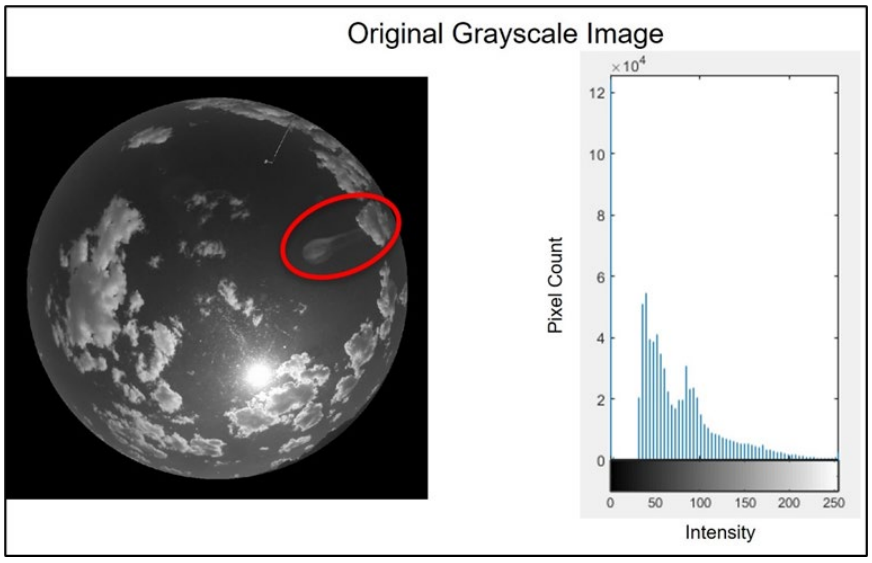

Fig. 19 CLAHE example: original grayscale image and histogram

Once the CLAHE is applied, see Fig. 20, the artifact and clouds are much clearer than the original image. This improved contrast provides an easier target for removing the non-cloud feature.

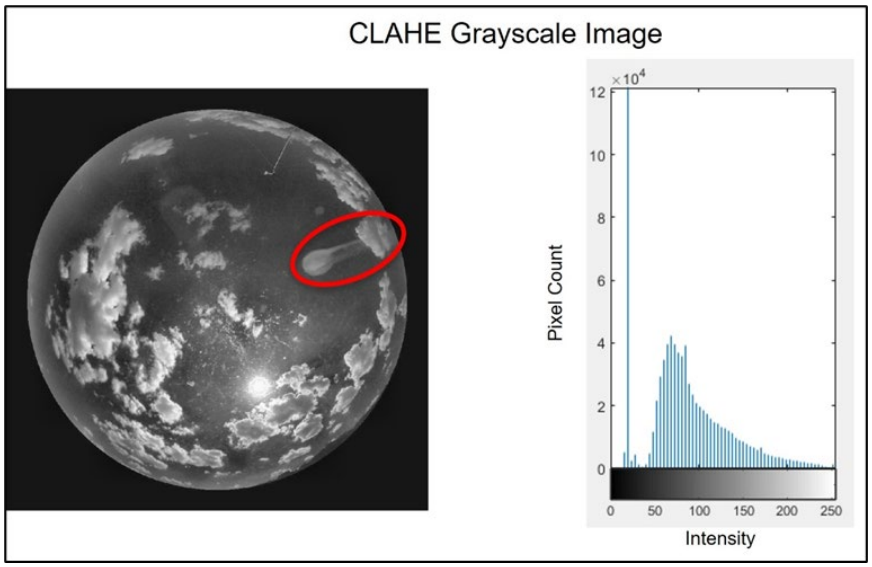

Fig. 20 CLAHE example: CLAHE processed image and histogram

4.3 Image Sharpening

A technique known as unsharp masking can be used to sharpen an image by taking a blurred, negative image to create a mask that is then combined with the original positive image (Sharpening: Unsharp Mask n.d.). Usually, a clearer image results, but may be a less accurate representation of the subject due to the creation of new

information. Too much sharpening can introduce different types of artifacts to the image. This pre-image analysis tool was considered for its ability to emphasize edges and demarcations within images. Figure 21 shows a before and after image sequence using the image sharpening function. The circled area highlights how the definition and clarity of the image was increased after using the tool. Wispy clouds gained better-defined edges and are easier to discern.

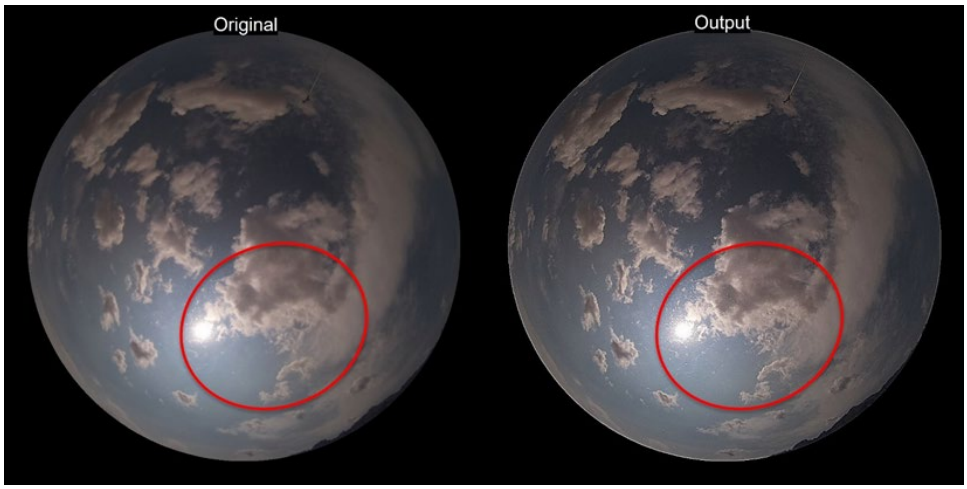

Fig. 21 Image sharpening example

4.4 Morphological Opening

The morphological opening tool erodes an image and then dilates it while using the same structuring element for both operations. Erosion removes floating pixels and thin lines, while dilation makes objects more visible and fills in small holes. Therefore, this tool was useful for removing small objects and thin lines while preserving the shape and size of larger objects within an image. This function was considered because it was effective at removing lens scratches and similar artifacts, especially from CLR sky images that tended to misinterpret lens scratches as thin clouds.

Figure 22 demonstrates the removal of lens scratches and a meteorological tripod rising over the horizon (see red circles), while maintaining the clear blue sky surrounding these artifacts. In contrast, Fig. 23 shows how the correction can also cause existing clouds to become “fuzzy” and unsuitable for quantification (see red circles).

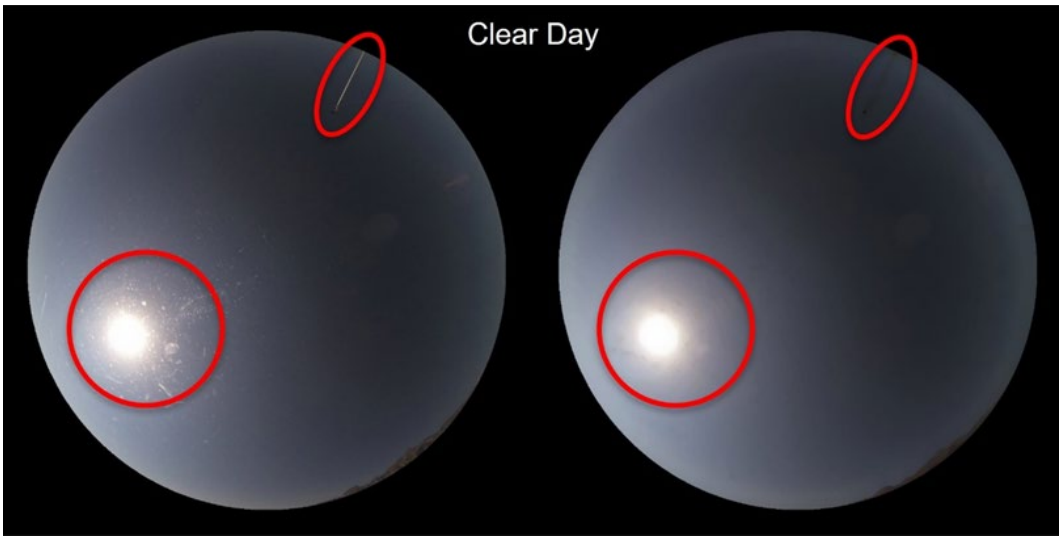

Fig. 22 Successful CLR morphological opening example

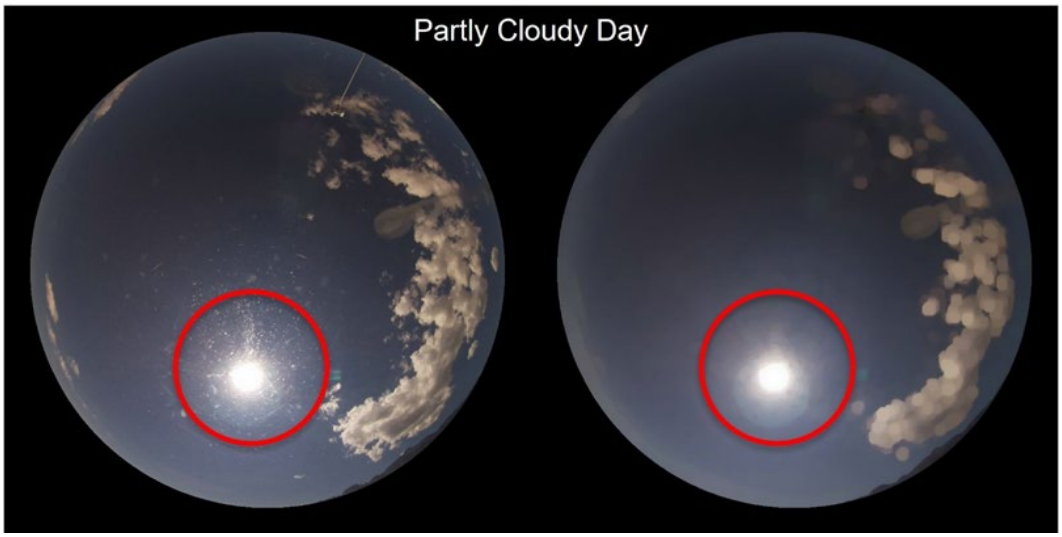

Fig. 23 Unsuccessful PC morphological opening example

4.5 Morphological Erosion

As mentioned earlier, morphological erosion is an operation that can be used to remove floating pixels and thin lines. The output pixel value is the minimum value of all the pixels in the neighborhood. Therefore, in a binary image (having only 0s and 1s), if any neighboring pixels have a 0 value, the pixel is set to 0. This tool was selected because it was very effective in removing lens scratches from PC sky images. Compared to morphological opening, this operation was slightly less efficient, but preserved the clarity of clouds and other details.

Figure 24 displays a morphological erosion example. The circled area demonstrates the effectiveness of removing artifacts with this operation. Most anomalies are removed, including the mast (top right of image), while the clouds remain the same.

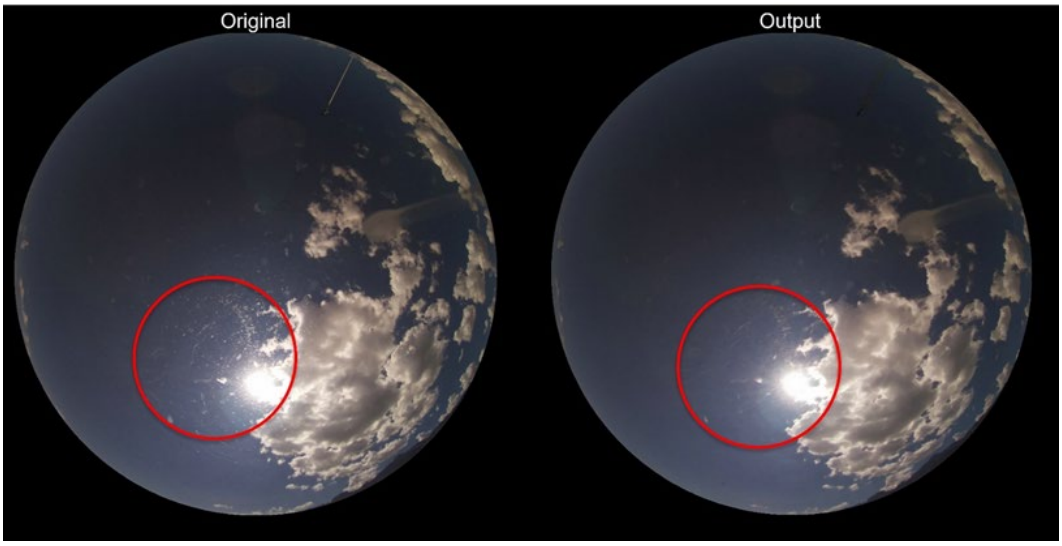

Fig. 24 Morphological erosion example preserves cloud detail

4.6 Edge Detection

The Edge Detection function uses image gradients to highlight and detect features such as edges and corners. A Sobel operator is used to detect the image's first derivative maximum and minimum. An approximation of the image intensity gradient function gives the direction of the largest possible increase from light to dark, and the rate of change, or how likely it represents an edge (Vincent and Folorunso 2009). Figure 25 shows the original and output from this function. In the output image, the cloud edges are clearly visible (along with the meteorological tower) and all optical artifacts are removed. Unfortunately, determining exactly where the clouds are located is difficult, and the cloud layers were removed. This tool was considered for its ability to detect and emphasize the edges of clouds.

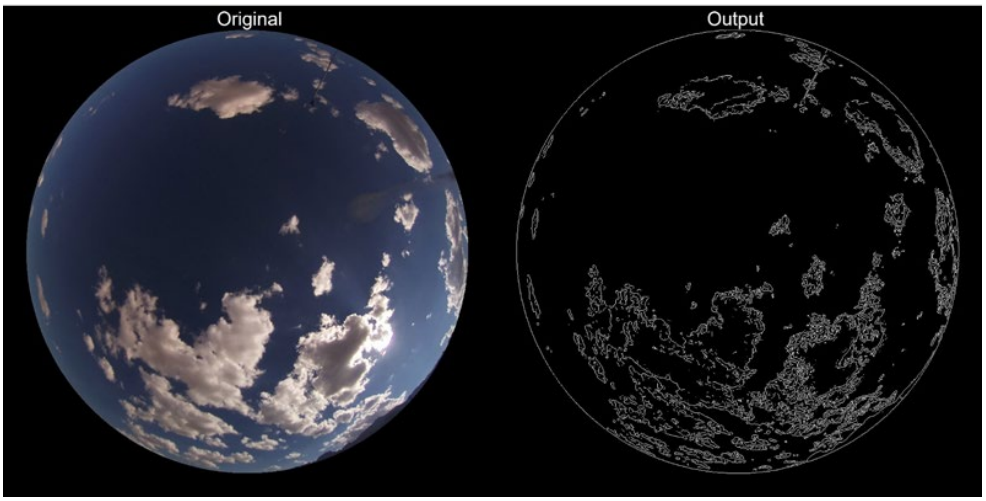

Fig. 25 Edge detection example

4.7 Inpainting

The Inpainting technique can restore, remove, or replace selected objects within an ROI. The function automatically fills in the region with information from the surrounding area (Bertalmio et al. 2000). This was selected to remove the sun-corona and artifacts using neighboring data. However, extraneous information can be introduced if the neighboring areas are not clear.

In Fig. 26, the top images are the originals while the bottom images show the post-inpainting output. The circled areas show how the sun's ROI was changed. For the OVC and first PC images, the function successfully removed the sun and replaced the area with blue sky. In the third image-set (PC on right), the sun ROI appears to the human eye to be surrounded by blue sky and the sun's radiance. However, the inpainting function picked up cloud cover in the ROI and replaced the sun pixels with "new" cloud pixels. In this later case, the function falsely increased the cloud pixel count, negating its usefulness for this scenario.

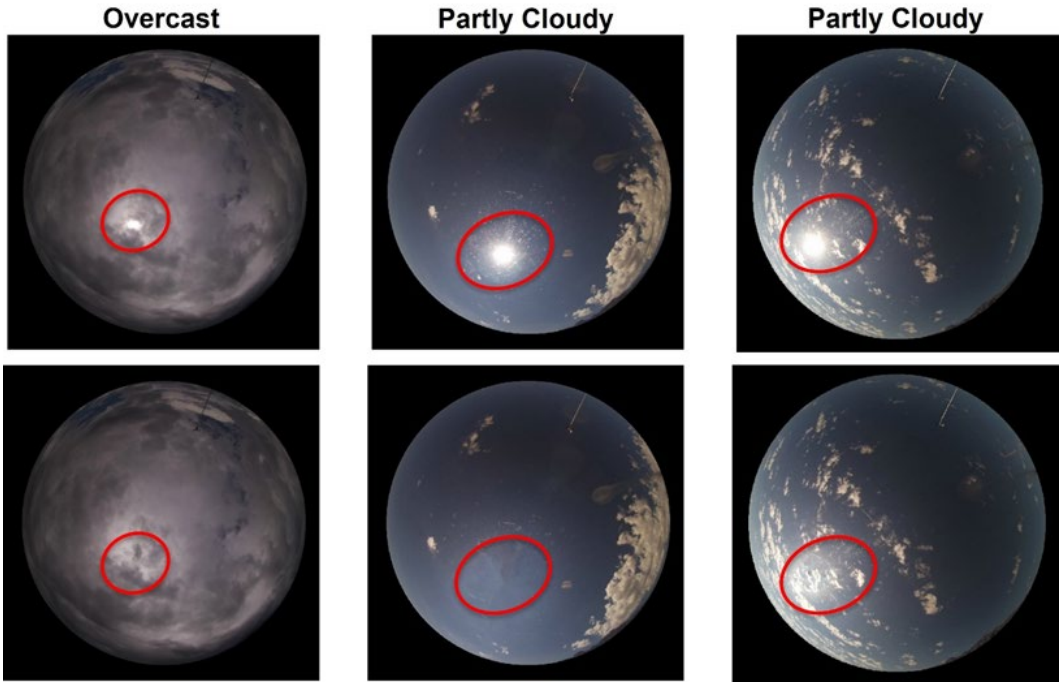

Fig. 26 Inpainting function replaces the sun with mixed results

4.8 Circle Detection

The Circle Detection function uses the Hough Transform technique to seek features specified in a parametric form. This function is most commonly used for the detection of regular curves such as lines and circles through their parametric equations (Young 2022). This tool was considered for its potential to detect raindrops on the WSI lens and to track weather changes.

In Fig. 27, two images were sampled on the same day, 15 min apart, to determine if the raindrops on the lens could be detected. Both images were processed using morphological opening, sharpening, adaptive histogram equalization, and an image gradient filter. Nearly all raindrops were detected using the circle detection function, enabling a better view of the dynamic raindrop distribution over time.

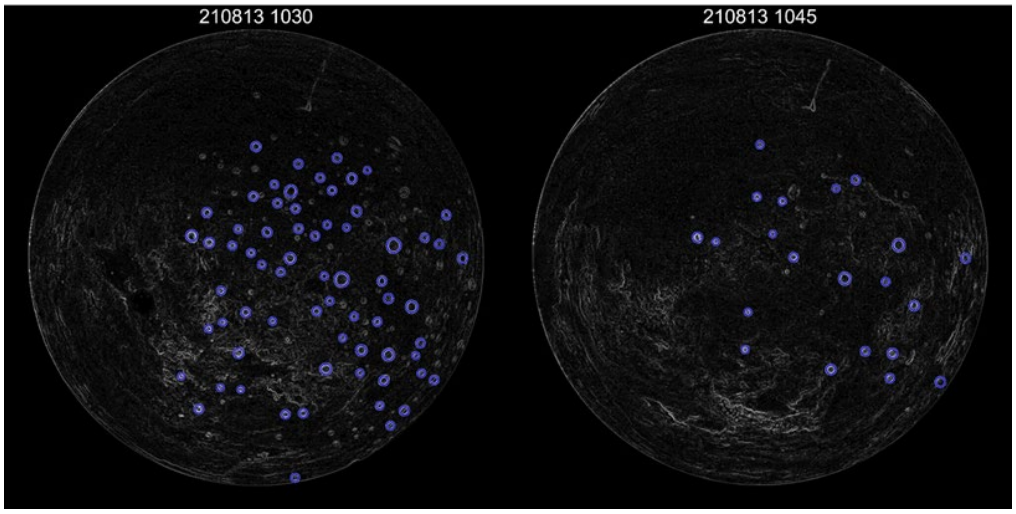

Fig. 27 Circle detection

4.9 Alternative Image Analysis Tools Summary

The most effective countermeasures for artifacts and enhancement were determined to be gamma correction, image sharpening, and morphological erosion. These tools had the least number of limitations and could be applied in tandem to generate the most constructive effect. Applying gamma correction first improved the contrast, before using the image sharpening to enhance details. The morphological opening was effective only during clear days due to its unwanted effect of blurring clouds and similar small details. On OVC days with rain, this function was effective in removing the raindrops but made the cloud layers indiscernible. Likewise, the use of inpainting to remove artifacts was successful only in certain conditions due to its tendency to introduce new information to the image. Edge detection was useful in detecting the cloud outlines but could not be used to its full potential because their actual locations were difficult to determine. Overall, these tools, despite certain limitations, showed potential for preparing whole sky images for further integration with the percent cloud cover determination.

5. Discussion: Cloud Characterization

The application of functions described in Section 4 were iteratively applied in the percent cloud algorithm development. In this section, a sample of the experimentation is described, along with a description of a refined assessment toward their usefulness to the algorithm development.

5.1 Gamma Correction and RGB Thresholding on OVC Images

Thin lines of blue sky in an OVC image can be difficult to detect. However, combining the gamma correction and RGB thresholding, these subtle features are revealed. Figure 28 displays an original OVC case image (top left), later evaluated as 9/10 cloud cover, gamma-corrected images (right side), and images with the adjusted RGB threshold (bottom images).

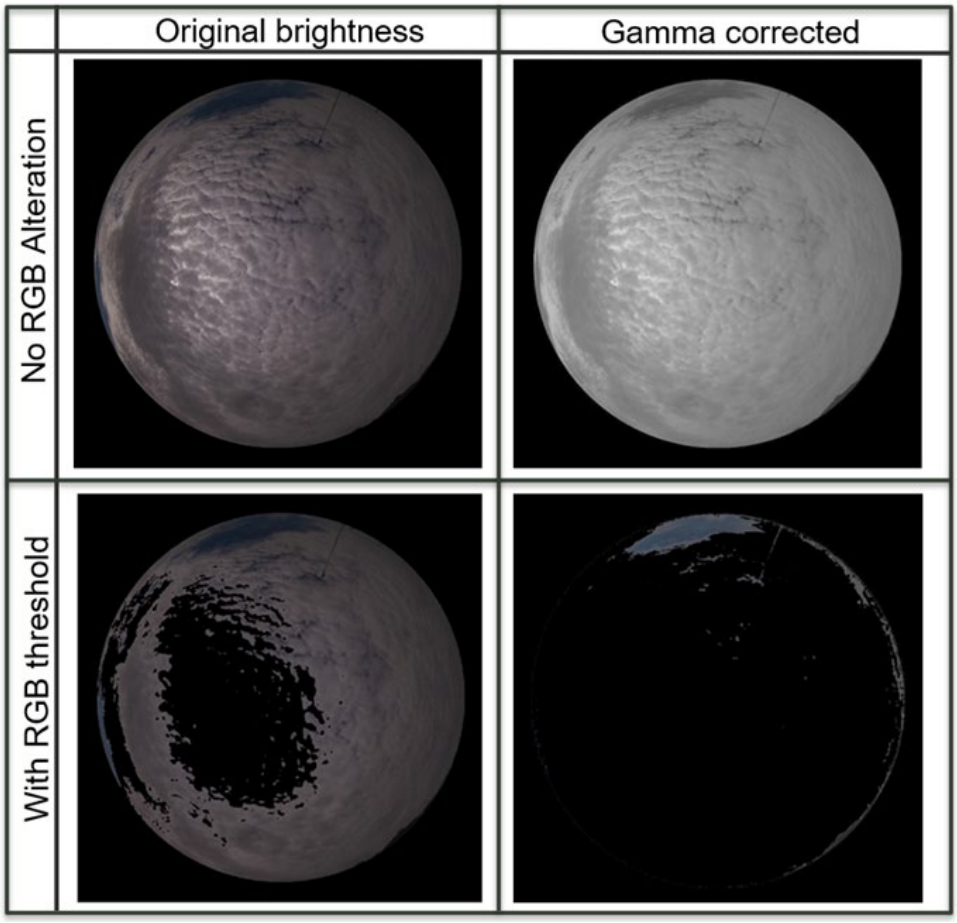

Fig. 28 Overcast RGB thresholding with gamma correction

To step from the original photo (top left) to the gamma-corrected status (top right), the histogram of the original image was right adjusted (Fig. 29). The source of the spikes introduced in the second histogram was unclear. It was noted that there was a billow structure within the image that was brought out by the improved contrast.

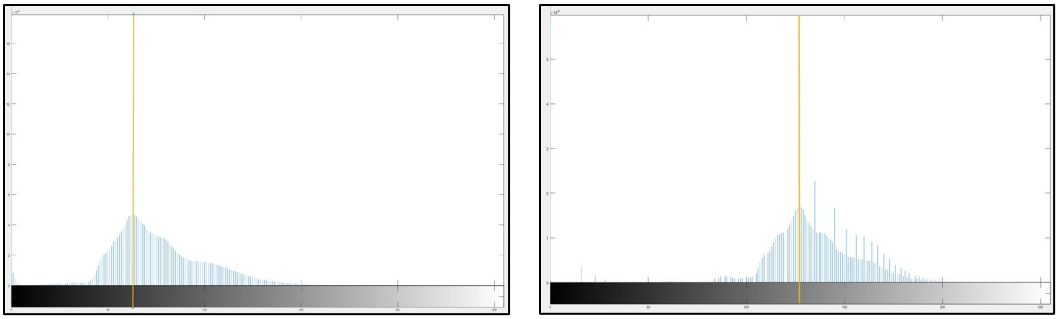

Fig. 29 Original (left) and gamma-corrected (right) image histogram

Even with an improved contrast, discerning blue sky was still not easily discerned. RBG thresholding was selected to "remove" the sun-brightened areas (Fig. 28, lower left), enabling better detailing of the non-sun/cloud mix areas. The "new" results were subjected to a gamma-correction (Fig. 28, lower right image). The more even color distribution exposed a small area of sky (10%) at the top of the image, which had been hard to interpret earlier.

5.2 Cloud Layer Detection

The initial cloud type analysis began by dividing the imaged clouds into three categories: top layer or cirrus, bottom layer or cumulus, and mid-layer or stratus. For simplicity, the mid- and lower layers were combined. Examples of the top layer/cirrus (Case 1), bottom layer/cumulus (Case 2), and a case that included two cloud layers (Case 3) are shown in Fig. 30. Masks were generated for each layer. The RGB threshold adjustment results are displayed in the bottom row of Fig. 30.

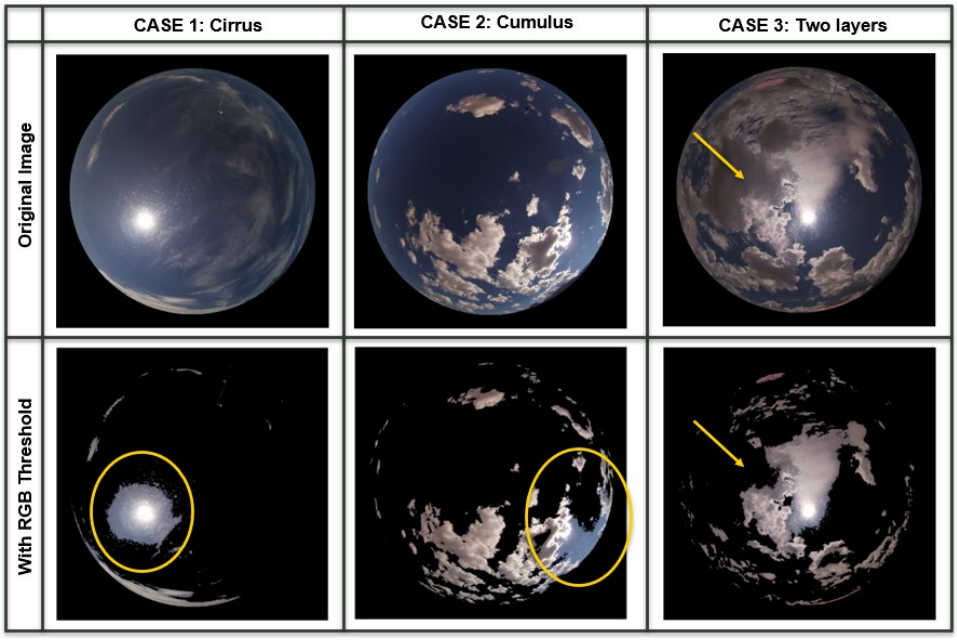

Fig. 30 PC RGB threshold, cloud layer results

Case 1 (top layer) results captured the cirrostratus, as well as the sun-corona. However, the thin, almost transparent wisps of cirrus eluded the thresholding.

The RGB thresholding was more successful at preserving the bottom/mid-layer cumulus, from Case 2. Unfortunately, there was a significant portion of blue sky that could not be eliminated (defined with 0 [black] values) with this same RGB threshold selection. After trial-and-error experimentation, this rogue blue sky was removed using the RGB thresholding technique; however, the updated "blue sky" threshold also eliminated cloud data from the image.

Case 3 represents the two-cloud layer image. The RGB thresholding results reported the same complications. For this example, a mask was created to remove the blue sky, inferring that the remaining total pixel count would represent the cloud cover in the test image. Unfortunately, the color contrasts between the thick clouds and the sky were close to one another. The blue sky thresholding also interpreted the dark cloud as "sky". This net effect is seen in Fig. 30, which shows the blue sky redefined as 0s, along with the darker cumulus cloud (yellow arrow ROI).

6. Summary and Conclusions

The initial quest of this research was to service an atmospheric model by developing an algorithm that could automatically analyze a WSI image and determine its percent cloud cover. This algorithm has been formulated. The preliminary results indicate that the process is worthy of a refinement and validation study. However,

one of the greater gems gleaned from this effort was correlating sun-corona pixel percentage and *sky* types. With the sky type intelligence, the ability to define the cloud layers and cloud types within the image is significantly advanced. For example, a CLR sky type indicates no clouds, maximizing the opportunity for SR to reach the PV panel. If an OVC sky type is defined, clouds are likely stratus or cumulus (low layer), strongly inhibiting (minimizing) SR from reaching the PV panel.

Focusing on the percent solar-corona investigation results, some of the key takeaways gleaned from the whole sky images sampled between 1000 and 1600 LT, during August through early October, include the following:

- The solar disc is closest to a circle (minimal percent sun-corona disc) at its highest point (zenith) under CLR sky conditions. The sun disc shape becomes an oval (larger percent magnitudes) as it nears the horizon, due to lens distortions. The highest sun position in the sky for the sampled case conditions occurred at 1300 MDT.
- For this study, the processed sky conditions were defined as follows:
    - CLR conditions include cloud cover <10%; with the sun not covered.
    - OVC conditions include cloud cover >90%; with sun covered.
    - PC conditions include cloud cover between 10% and 90%; sun may or may not be covered by thin or thick clouds.
- CLR sky conditions generated percent sun disc magnitudes between 0.20% and 0.55%, with an average value of 0.30%, and a minimum/maximum spread of approximately 0.2%.
- OVC sky conditions generated percent magnitudes between 0.00% and 0.26%, with an average value of 0.03%.
- PC sky conditions varied greatly. Using an unfiltered data resource, PC sky generated percent magnitudes between 0.10% and 1.71%, with an average value of 0.36%. After removing near OVC, no sun and thick clouds, the minimum/maximum percent sun disc spread was between 0.2% and 0.4%.
- PC conditions were divided into thin and thick cloud types covering the sun disc. The thick cloud occultation produced results that imitated OVC sky conditions. The thin cloud occultation showed a scattered version of almost CLR sky magnitudes when displayed as a function of time.

- Special cases:
    - OVC with the sun behind thin clouds leaned toward PC/CLR results.
    - PC with the sun positioned in blue sky (no cloud filtering the direct solar energy) tended to imitate CLR results.

The percent cloud algorithm has several opportunities for exploiting the percent sun-corona disc results.

- For the CLR sky cases: Due to the well-behaved nature of the sun disc pixel count, an automated routine finding the percent sun-corona disc within a CLR sky range could use the RGB threshold to confirm the absence of clouds, then issue the 0% clouds, 100% blue sky output.
- For OVC conditions: The competitive condition for the 0%–0.3% is the PC *without* a sun disc. Here the RBG threshold would be helpful to verify the presence of cloud cover and its extent.
- For PC sky: The impact of thick and thin clouds over the sun of a PC sky remains a challenge. While several possible approaches were considered, including using RGB to take the more difficult blue sky pixels, the outputs were not conclusive.

In conclusion, the research conducted has improved the understanding of RGB thresholding with respect to whole sky image analysis capabilities, and it has contributed to the ARL testbed by working to bridge the gap between the WSI analysis and the SR model. As the process becomes more precise and accurate, the ability to integrate solar fuels into the hybridized tactical and civilian power resources improves, thus reducing warfighter vulnerabilities to enemy forces or disaster relief emergency personnel to powerless environments. Optimized power reduces fuel truck convoy resupply requirements that serve as a target for enemy forces and logistical delays for civilians. Additionally, it reduces logistical footprints in isolated operating areas. Applying image processing techniques to tactical and civilian applications opens opportunities to enhancements in reconnaissance, communications and even for medical imaging analyses (see Appendix G). In the next section, several recommendations are provided.

7. Recommendations

The potential for future investigations stemming from this research are numerous. A list of just some of these opportunities follows:

- Image lighting is, in part, a function of the sun's position in the sky. Use histograms to adapt image light distribution, based on solar position.
- Experiment with histogram distributions to determine if a gamma correction and/or other image analysis functions should be applied.
- Link gamma correction with image exposures.
- Use artificial intelligence to develop recognition of repeated artifact patterns and to possibly predict sky/cloud patterns.
- Refine the cloud cover assessment by creating more than one binary mask for an ROI to a specific subject (e.g., clouds and sun).

Finally, it is recommended to continue a strategy begun in this study, namely, shifting the analysis target from clouds to blue sky. Detecting blue sky would provide only total cloud cover, and not top and bottom cloud layer quantities. However, using an inverse image on the "total cloud cover," the extracted results could bring the cloud layer slicing into a more fruitful, detailed opportunity.

8. References

Altocumulus. Glossary of Meteorology, American Meteorological Society (AMS); n.d. [accessed 2022 Aug 12]. https://glossary.ametsoc.org/wiki/Altocumulus.

Altostratus. Glossary of Meteorology, American Meteorological Society (AMS); n.d. [accessed 2022 Aug 12]. https://glossary.ametsoc.org/wiki/Altostratus.

Bertalmio M, Sapiro G, Caselles V, Ballester C. Image inpainting. Proceedings of the 27th Annual Conference on Computer Graphics and Interactive Techniques. July 2000;417–424. https://doi.org/https://doi.org/10.1145/344779.344972.

Ceiling. Glossary of Meteorology, American Meteorological Society (AMS); n.d. [accessed 2022 Aug 12]. https://glossary.ametsoc.org/wiki/Ceiling.

Cloud Classification. Glossary of Meteorology, American Meteorological Society (AMS); n.d. [accessed 2022 Aug 12]. https://glossary.ametsoc.org/wiki/Cloud_classification.

Cumulus. Glossary of Meteorology, American Meteorological Society (AMS); n.d. [accessed 2022 Aug 12]. https://glossary.ametsoc.org/wiki/Cumulus.

Fulton W. What and why is gamma correction in photo images? ScanTips. [accessed 2022 Aug 12]. www.scantips.com/lights/gamma2.html.

Halo of 22°. Glossary of Meteorology, American Meteorological Society (AMS); n.d. [accessed 2022 Aug 12]. https://glossary.ametsoc.org/wiki/Halo_of_22%C2%B0.

Huamán A. Histogram equalization. OpenCV. https://docs.opencv.org/4.x/d4/d1b/tutorial_histogram_equalization.html.

Image Quality Factors White Balance. Image Engineering; c2022 [accessed 2022 Aug 12]. https://www.image-engineering.de/library/image-quality/factors/1079-white-balance.

Liou K-N. An introduction to atmospheric radiation. Academic Press; 1980.

Magurno D, Cossich W, Maestri T, Bantges R, Brindley H, Fox S, Harlow C, Murray J, Pickering J, Warwick L, et al. Cirrus cloud identification from airborne far-infrared and mid-infrared spectra. Remote Sensing. 30 June 2020;12(13):1–19. https://doi.org/10.3390/rs12132097.

Nimbostratus. Glossary of Meteorology, American Meteorological Society (AMS); n.d. [accessed 2022 Aug 12]. https://glossary.ametsoc.org/wiki/Nimbostratus.

Sharpening: Unsharp Mask. Cambridge in Colour; n.d. [accessed 2022 Aug 12]. https://www.cambridgeincolour.com/tutorials/unsharp-mask.htm.

Skyvue8 - Lidar Ceilometer. SkyVUE8: LIDAR Ceilometer. Campbell Scientific; n.d. [accessed 2022 Aug 12]. https://www.campbellsci.com/skyvue8.

US Department of Commerce. Cloud Classification. National Weather Service, National Oceanic and Atmospheric Administration (NOAA); 2020 May 30. https://www.weather.gov/lmk/cloud_classification.

Vaucher G, Lee MS, Goodman H. In-situ atmospheric intelligence for hybrid power grids: Volume 3 (analysis of whole sky image compression). DEVCOM Army Research Laboratory (US); 2021 Dec. Report No.: ARL-TR-9360.

Vaucher G, Randall R, Bergen S, Jane R. Atmospheric intelligence for hybrid power advancements: Volume 1 (wind impacts on photovoltaic power/panel temperature). DEVCOM Army Research Laboratory (US); 2023 Jan. Report No.: ARL-TR-9629.

Vincent O, Folorunso O. A descriptive algorithm for Sobel image edge detection. InSITE Conference; 2009. https://doi.org/10.28945/3351.

Young D. Hough transform for circles. MATLAB Central File Exchange; 2022. https://www.mathworks.com/matlabcentral/fileexchange/26978-hough-transform-for-circles.

Appendix A. WSI Image Examples by Sky Type (15) and Special Cases (2)

Appendix A contains examples of the whole sky image data used for this report's research analyses. These data files were acquired over a southwestern, New Mexico, location called "Site B". The displayed images were taken at 1300 MDT and provide a mid-sunlight day snapshot of the five Clear (Fig. A-1), five Overcast (Fig. A-2), and five Partly Cloudy (Fig. A-3) cases discussed in the technical report. Two sequenced special case images (Fig. A-4) show a 22° halo as part of the 2021 September 25 Overcast case at Site B.

Photos are aligned so that north is up, and east is to the left. The diurnal solar path traverses the image from left (east) to right (west). Date labels/captions for each image are in a 2-digit year, month, day (YYMMDD) format. For additional information, see Section 1.3 and Table 1 of the main report.

(a) 210826, 1300 MDT

(b) 210910, 1300 MDT

(c) 210914, 1300 MDT

(d) 210917, 1300 MDT

(e) 210921, 1300 MDT

Fig. A-1 Five clear sky cases: site B (2021)

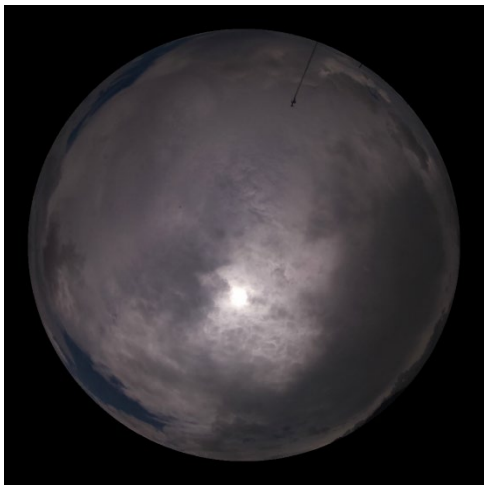

(a) 210813, 1300 MDT

(b) 210814, 1300 MDT

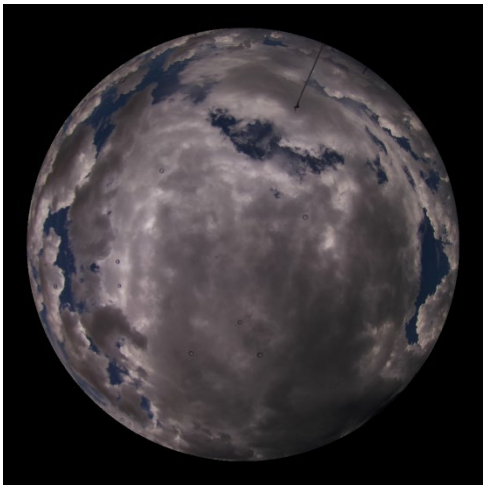

(c) 210902, 1300 MDT

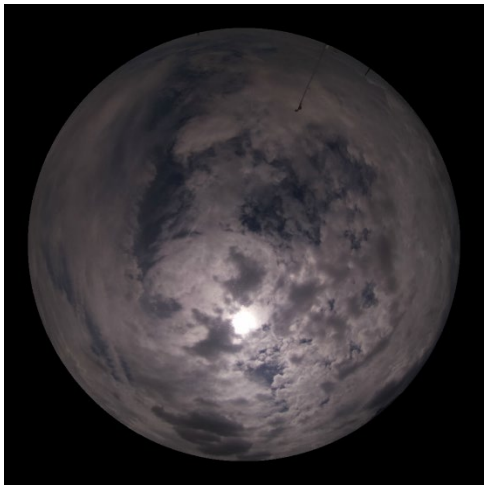

(d) 210905, 1300 MDT

(e) 210925, 1300 MDT

Fig. A-2 Five overcast sky cases: site B (2021)

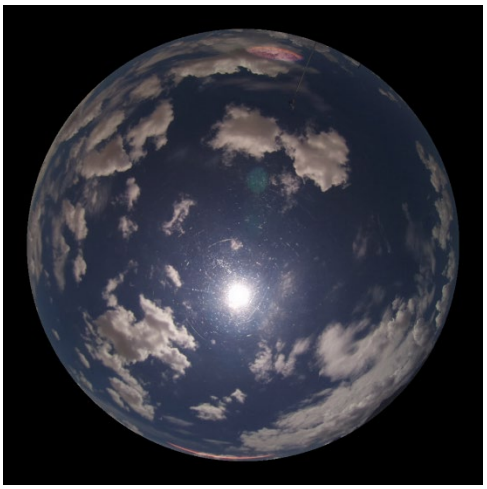

(a) 210812, 1300 MDT

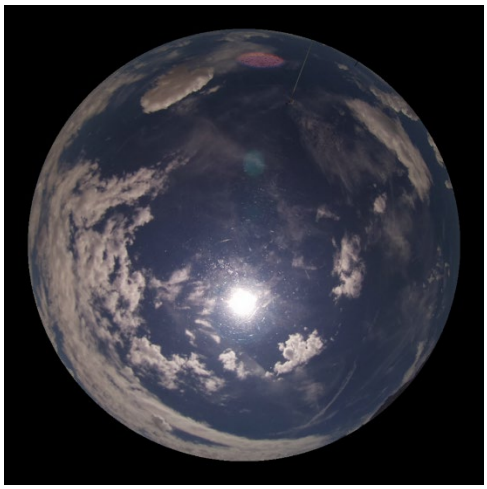

(b) 210821, 1300 MDT

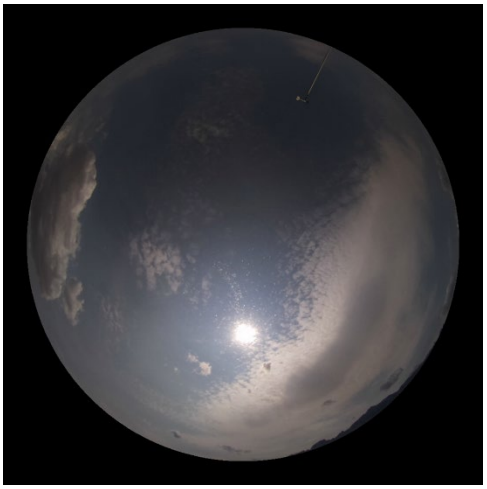

(c) 210927, 1300 MDT

(d) 211001, 1300 MDT

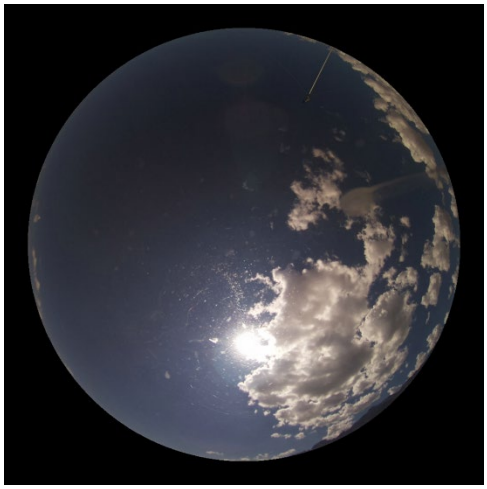

(e) 211006, 1300 MDT

Fig. A-3 Five partly cloudy sky cases: site B (2021)

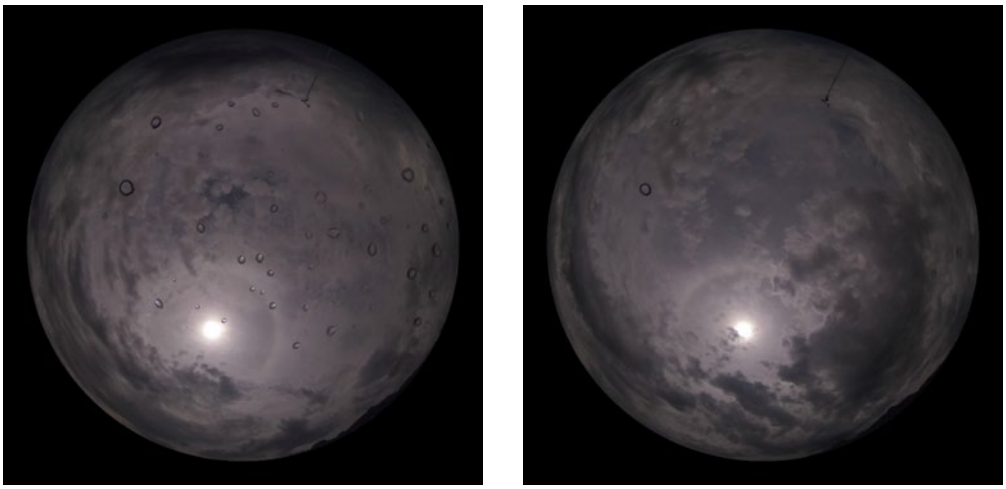

(a) 210925, 1215 MDT (b) 210925, 1230 MDT

Fig. A-4 Two OVC special cases: 22° halo over site B (2021)

Appendix B. Percent Sun Disc Algorithm Tutorial

This appendix appears in its original form, without editorial change.

The Percent Sun Disc Algorithm Tutorial explains the procedure for determining the percent pixel count of the sun-corona, with respect to the Whole Sky Imager image. The same method can be applied to determining percent cloud cover.

Program: PercentSunCorona_Algorithm (MATLAB R2022a)
Last updated: 2023 Jan 31
Author: Goodman and Vaucher.

PURPOSE: To determine the percent of pixels comprising the solar disc and its corona with respect to the total circular, whole sky image. This method is also applicable to determining percent of clouds in a sky image.

Step 1. Image Segmenter – Determine the total pixels (denominator) contained in the circular sky portion of the Whole Sky Imager (WSI) image.

Overview: The original rectangular WSI photograph contains a black frame outside of a circular sky image. To eliminate the pixel count of this frame, the Image Segmenter isolates the sky circle, converts those pixels into '1s' (made white), while the portion outside the circle is labelled as '0s'. The total pixel count or area within the circle (denominator) is tallied by counting the 1s.

Optional Step: As an independent check, the diameter of the sky circle (non-black frame) can be determined using the Image Segmenter; the diameter is converted into a radius and the area (pixel count) is calculated using:

$$\text{Area} = \text{pi} * (\text{diameter}/2)^2. \qquad \text{(B-1)}$$

Step 1.1 Image Segmenter – Isolate the circular sky-portion of image and convert those pixels into '1s' (seen as a white color).

1.1.1 Open MATLAB R2022a; select "APPS" at the top of the MATLAB window.

1.1.2 Select "APPS" at the top, then,

Locate the "Image Process and Computer Vision" functions, and

Select "Image Segmenter" (a new window will appear).

1.1.3 Select "load image" then, "load image from file".

1.1.4 Select the subject image, then "Open". Wait for image to appear.

1.1.5 Under "Add to Mask", select "draw ROI" (ROI = region of interest).

1.1.6. Select "circle" and spread a circle over the entire sky portion of the image. The 'preview' result should look like the images below. On the left is a Clear case; on the right is a partly cloudy example.

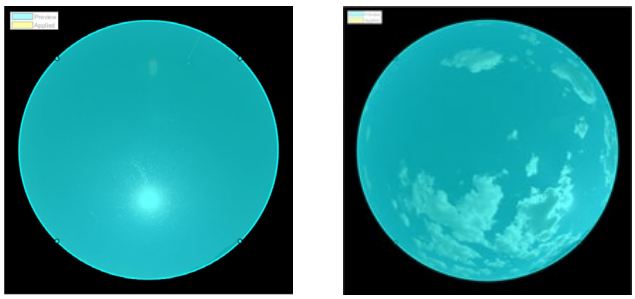

1.1.7. Click "Show Binary" and "Apply". Sky circle should turn white (1s) and the frame remain black (0s) (see figure below):

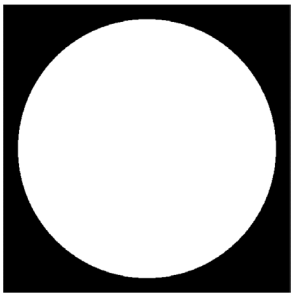

1.1.8. Click "Close ROI".

Step 1.2 Image Segmenter – Save the circle images.

1.2.1 Select "Export", "Export Images".

1.2.2 In the "Export to Worksheet" window:

Check both boxes ("Final Segmentation" and "Masked Image").

Fill in "BW**1**" for top box, and "maskedimage**1**" for the bottom box; and

Click "Ok".

1.2.3 The Workspace should now list 2 entries: "BW1" and "maskedImage1".

1.2.4. Close the Image Segmenter window, if you are not doing the optional Step 1.3.

Step 1.3 (Optional Step): Image Segmenter – To automate process: Save as a function:

1.3.1 Click "Export" (to right of 'show binary'), then

1.3.2 Select "Generate Function".

1.3.3 Save function by naming it.

Step 1.4 (Optional step): Image Segmenter – Independently validating WSI image's circular sky pixel count using its diameter. This is an optional independent method for calculating an estimated pixel number within the circle.

1.4.1 Open MATLAB R2022a; select "APPS" at the top of the MATLAB window.

1.4.2 Select "APPS" at the top, then,

Locate the "Image Process and Computer Vision" functions, and

Select "Image Segmenter" (a new window will appear).

1.4.3 Select "load image" then, "load image from file".

1.4.4 Select the subject image, then "Open". Wait for image to appear.

1.4.5 Under "Create Mask", select "find circles".

1.4.6 Select 'Ruler' (top left); With the mouse, draw a straight line across the circular sky image, to determine the number of pixels represented in the circle's diameter. Note Land on the perimeter could cause results to differ from the circle method.

1.4.7 Insert circles diameter into the circle area/pixel count equation:

Example:	Diameter = 915 pixels.
Equation:	Area = pi * (diameter/2)^2.
Results:	657555 pixels.

Step 2. Color Thresholder: Extract solar disc portion of the image (numerator).

In Step 2, the total pixel count for the sun disc and its corona is determined by creating a binary mask for this sun footprint using the color thresholder feature. This binary array serves as the numerator for the final calculation. Note that this procedure can also be used to determine cloud pixel count (once the sun pixel total of Step1, is determined).

2.1 Select "APPS" at the top of the MATLAB window, then

Locate the "Image Process and Computer Vision" functions, and

Select "Color Thresholder" (a new window will appear).

2.2 Select "Load Image"; "Load image from file" (select same image used in Step 1).

2.3 Select "RGB"

Adjust Red threshold (move the right side, blue rectangle slider box to the left) to include only (0 – 225);

Leave green and blue at default (removing high intensity red pixels only)

Results should look similar to the image that follows:

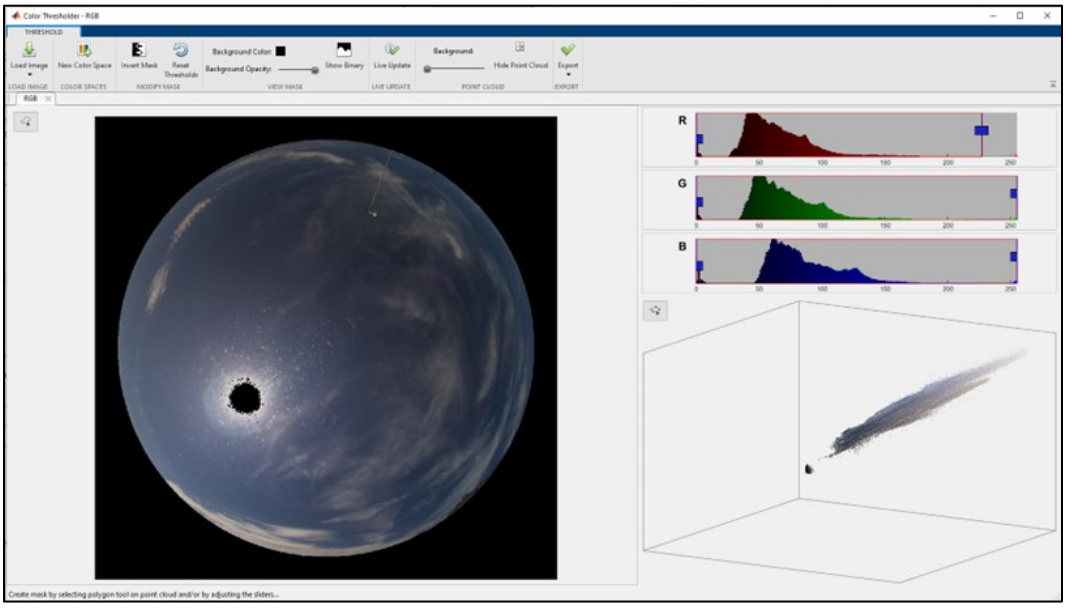

2.4 Select “Show Binary”, then “Invert Mask” – now the sun and corona are all 1s (white).

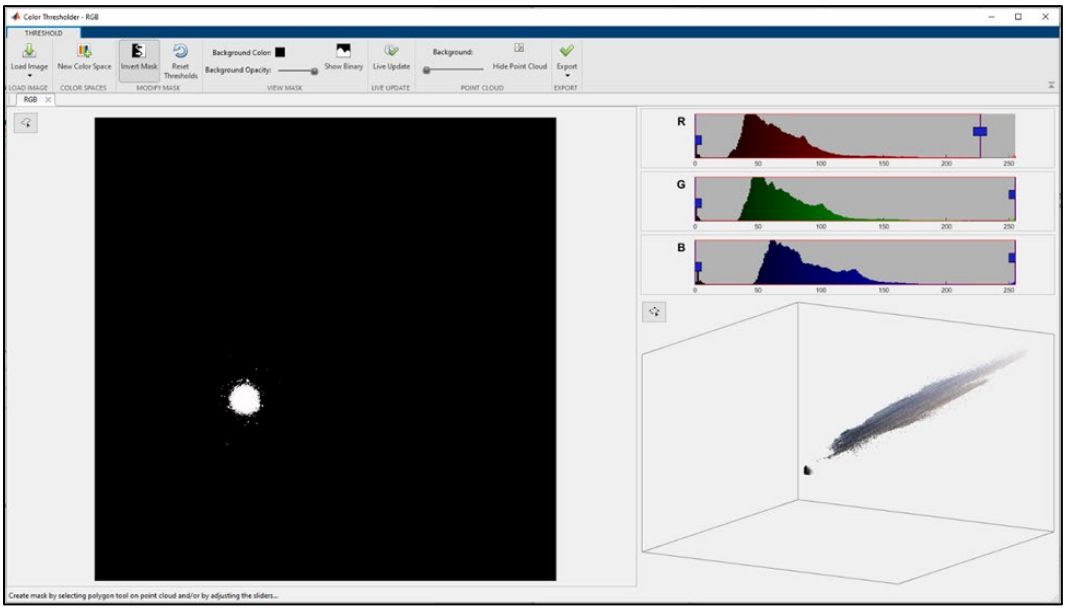

2.5 Select “Export”, then “Export images”

2.5.1 Ensure all check boxes are selected.

2.5.2. Name “Binary Mask” : “BW**2**”

2.5.3. Name “Masked RGB image” : “maskedRGBimage**2**”

2.5.4. Name “Input RGB Image”: inputImage**2** (or leave as default).

2.5.5. Select “ok”.

2.6 To save steps as a function, select “Export” then “Export Function”.

2.7 Close “Color Thresholder” window.

2.8 The Workspace should now list 5 entries:

“BW1” and “maskedImage1”.

“BW2, “maskedImage2”, and “maskedRFBImage2”.

Step 3 - Image Region Analyzer: Determine the image’s solar disc/corona percent by comparing the sun-corona pixel count, to the total sky pixel count.

3.1 In the MATLAB command line, PercentSunPixelCount = nnz(BW2)/nnz(BW1) * 100

3.2 To manually check pixel numbers:

3.2.1 Select “APPS” at the top, then

Locate the “Image Process and Computer Vision” functions, and

Select “Image Region Analyzer” (a new window will appear).

3.2.2 Select “Load Image” then “Load Image from Workspace”.

3.2.3 BW1-Total Image Pixel Count:

- Select “BW1” (workspace sun exported by Color Thresholder), then “ok”.
- Highlight “Area” column to turn the white pixels into a peach color on the displayed image. Visually confirm the workspace image is representing the Total whole sky image. Turn off the peach color by clicking outside the Area column.
- Select “Choose Properties”, check only “Area”.
- Select “Export”; select “export properties”; label output as propsStruct1, propsTable1. The latter is a table that can be copied into an excel spreadsheet. Tally the Area column to determine pixel count for the total sky image, which should equal the number in cell 1x1 in propsTable1:

$$\text{Image\_Total} = \text{nnz}(\text{BW1}). \qquad \text{(B-2)}$$

3.2.4 BW2-SunCorona Pixel Count:

- Return to Image Region Analyzer, Load Image from workspace,
- Select “BW2” (workspace sun exported by Color Thresholder), then “ok”.
- Highlight “Area” column to turn the white pixels into a peach color on the displayed image. Visually confirm the workspace image is representing the solar disc and corona. Turn off the peach color by clicking outside the Area column.
- Select “Choose Properties”, check only “Area”.
- Select “Export”; select “export properties”; label output as propsStruct2, propsTable2. The latter is a table that can be copied into an excel spreadsheet. Tally the Area column to determine pixel count for the total sun-corona pixel count, which should equal:

$$\text{SunCorona\_Total} = \text{nnz}(\text{BW2}). \qquad \text{(B-3)}$$

3.2.5 Percent sun shown in sky:

- Check_PercentSun = (SunCorona_Total / Image_Total) * 100%
  PercentSunPixelCount = nnz(BW2)/nnz(BW1) * 100
- **VALIDATION CHECK**:
  - DidItWork = (PercentSunPixelCount - Check_PercentSun)
  - If DidItWork = 0, it was successful!

Appendix C. Total Sky Function (Step 1)

This appendix includes the Step1_CLR_segmentImage(RGB) function for Clear sky cases. This function was used to determine the total pixel count of the sky image (no frame). Results are preserved in variables called BW1 and maskedImage1. To run this function, type

```
RGB = imread('photo.jpg');

[BW1, maskedImage1 ] = Step1_segmentImage(RGB);
```

The number 1 designates the denominator (total sky image pixel count) entry in the final percent equation.

Code provided by coauthor Hailey Goodman.

Function: Step1_CLR_segmentImage(RGB)

```
function [BW1,maskedImage1] = Step1_CLR_segmentImage(RGB)
%  [BW1,maskedImage1] = Step1_segmentImage(RGB) segments image RGB
%  using auto-generated code from the imageSegmenter app. The final segmentation
%  is returned in BW1, and a masked image is returned in maskedImage1.

% Auto-generated by imageSegmenter app on 31-Jan-2023
%----------------------------------------------------

% Convert RGB image into L*a*b* color space.
X = rgb2lab(RGB);

% Create empty mask.
BW1 = false(size(X,1),size(X,2));

% Draw ROIs
xPos = [970.4177 970.0625 968.9975 967.2244 964.7459 961.5657 957.6889 953.1214
947.8701 941.9433 935.3501 928.1006 920.2060 911.6785 902.5312 892.7782 882.4346
871.5164 860.0402 848.0240 835.4861 822.4459 808.9236 794.9399 780.5164 765.6754
750.4398 734.8330 718.8792 702.6028 686.0290 669.1835 652.0920 634.7810 617.2773
599.6077 581.7995 563.8802 545.8774 527.8189 509.7324 491.6460 473.5875 455.5847
437.6654 419.8572 402.1876 384.6838 367.3729 350.2814 333.4358 316.8621 300.5857
284.6318 269.0251 253.7894 238.9484 224.5250 210.5413 197.0189 183.9788 171.4409
159.4246 147.9485 137.0302 126.6866 116.9337 107.7864 99.2589 91.3643 84.1148
77.5215 71.5947 66.3435 61.7760 57.8991 54.7190 52.2404 50.4673 49.4024 49.0472
49.4024 50.4673 52.2404 54.7190 57.8991 61.7760 66.3435 71.5947 77.5215 84.1148
91.3643 99.2589 107.7864 116.9337 126.6866 137.0302 147.9485 159.4246 171.4409
183.9788 197.0189 210.5413 224.5250 238.9484 253.7894 269.0251 284.6318 300.5857
316.8621 333.4358 350.2814 367.3729 384.6838 402.1876 419.8572 437.6654 455.5847
473.5875 491.6460 509.7324 527.8189 545.8774 563.8802 581.7995 599.6077 617.2773
634.7810 652.0920 669.1835 686.0290 702.6028 718.8792 734.8330 750.4398 765.6754
780.5164 794.9399 808.9236 822.4459 835.4861 848.0240 860.0402 871.5164 882.4346
892.7782 902.5312 911.6785 920.2060 928.1006 935.3501 941.9433 947.8701 953.1214
957.6889 961.5657 964.7459 967.2244 968.9975 970.0625 970.4177];

yPos = [514.3450 532.4315 550.4900 568.4928 586.4121 604.2203 621.8899 639.3937
656.7046 673.7961 690.6417 707.2154 723.4918 739.4456 755.0524 770.2881 785.1290
799.5525 813.5362 827.0585 840.0987 852.6366 864.6529 876.1290 887.0472 897.3908
907.1438 916.2911 924.8186 932.7132 939.9627 946.5560 952.4828 957.7340 962.3015
966.1784 969.3585 971.8370 973.6102 974.6751 975.0303 974.6751 973.6102 971.8370
969.3585 966.1784 962.3015 957.7340 952.4828 946.5560 939.9627 932.7132 924.8186
916.2911 907.1438 897.3908 887.0472 876.1290 864.6529 852.6366 840.0987 827.0585
813.5362 799.5525 785.1290 770.2881 755.0524 739.4456 723.4918 707.2154 690.6417
673.7961 656.7046 639.3937 621.8899 604.2203 586.4121 568.4928 550.4900 532.4315
514.3450 496.2586 478.2001 460.1973 442.2780 424.4698 406.8002 389.2964 371.9855
354.8940 338.0484 321.4747 305.1983 289.2444 273.6377 258.4020 243.5611 229.1376
215.1539 201.6316 188.5914 176.0535 164.0372 152.5611 141.6429 131.2993 121.5463
112.3990 103.8715 95.9769 88.7274 82.1341 76.2073 70.9561 66.3886 62.5117 59.3316
56.8531 55.0799 54.0150 53.6598 54.0150 55.0799 56.8531 59.3316 62.5117 66.3886
70.9561 76.2073 82.1341 88.7274 95.9769 103.8715 112.3990 121.5463 131.2993
```

```
141.6429 152.5611 164.0372 176.0535 188.5914 201.6316 215.1539 229.1376 243.5611
258.4020 273.6377 289.2444 305.1983 321.4747 338.0484 354.8940 371.9855 389.2964
406.8002 424.4698 442.2780 460.1973 478.2001 496.2586 514.3450];

m = size(BW1, 1);
n = size(BW1, 2);
addedRegion = poly2mask(xPos, yPos, m, n);
BW1 = BW1 | addedRegion;

% Create masked image.
maskedImage1 = RGB;
maskedImage1(repmat(~BW1,[1 1 3])) = 0;
end
```

Appendix D. Total Sun-Corona Function (Step 2)

This appendix includes the Step2_CLR_ColorThresholder_sun function for Clear sky cases. This function isolates the sun and corona pixels from the rest of the sky image, storing results in variable named: BW2 and maskedRGBImage2. To run this function, type

RGB = imread('photo.jpg');

[BW2, maskedImage2] = Step2_CLR_ColorThresholder_sun(RGB);

The number 2 designates the numerator (total sun and corona pixel count) entry for the final percent equation.

Code provided by coauthor Hailey Goodman.

Function: Step2_CLR_SolarThresholder_sun(RGB)

```
function [BW2,maskedRGBImage2] = Step2_CLR_ColorThresholder_sun(RGB)
%  OLD NAME: function [BW2,maskedRGBImage2] = createMask(RGB)
%  [BW2, maskedRGBImage2] = Step2_CLR_ColorThresholder_sun(RGB) thresholds
%  image RGB using auto-generated code from colorThresholder app.
%  The colorspace and range for each channel of the colorspace were set
%  within the app. The segmentation mask is returned in BW2, and a
%  composite of the mask and original RGB images is returned in
%  maskedRGBImage2.

% Auto-generated by colorThresholder app on 31-Jan-2023
%------------------------------------------------------


% Convert RGB image to chosen color space
I = RGB;

% Define thresholds for channel 1 based on histogram settings
channel1Min = 0.000;
channel1Max = 225.000;

% Define thresholds for channel 2 based on histogram settings
channel2Min = 0.000;
channel2Max = 255.000;

% Define thresholds for channel 3 based on histogram settings
channel3Min = 0.000;
channel3Max = 255.000;

% Create mask based on chosen histogram thresholds
sliderBW2 = (I(:,:,1) >= channel1Min ) & (I(:,:,1) <= channel1Max) & ...
   (I(:,:,2) >= channel2Min ) & (I(:,:,2) <= channel2Max) & ...
   (I(:,:,3) >= channel3Min ) & (I(:,:,3) <= channel3Max);
BW2 = sliderBW2;

% Invert mask
BW2 = ~BW2;

% Initialize output masked image based on input image.
maskedRGBImage2 = RGB;

% Set background pixels where BW is false to zero.
maskedRGBImage2(repmat(~BW2,[1 1 3])) = 0;

end
```

Appendix E. Percent Sun-Corona Function (Step 3)

The percent sun-corona cover is determined using total pixel count of the sun, divided by the total pixel count of the whole sky image:

a = (nnz(BW2) / nnz(BW1)) * 100;

Code provided by coauthor Hailey Goodman.

```
function [a, BW2, properties, sun, remainingarea] =filterRegions(BW1)
% function [a, BW2,properties, whitepixs, cloudpixs, sunpixs,CC] = filterRegions(BW1)
%filterRegions Filter BW image using auto-generated code from imageRegionAnalyzer app.

% Auto-generated by imageRegionAnalyzer app on 13-Jul-2022
%-----------------------------------------------------

BW2 = BW1;

% Get properties.
properties = regionprops(BW2, {'Area', 'Eccentricity', 'EquivDiameter', 'EulerNumber', 'MajorAxisLength', 'MinorAxisLength', 'Orientation', 'Perimeter'});
% determiene the percent of pixels in the image that are nonzero (nonzero =
% white pixels)
a = (nnz(BW2)/numel(BW1))*100;

end
```

Appendix F. Percent Cloud Cover Function (Step 4)

The Percent Cloud Cover algorithm uses the cloud cover and total sky pixel count to determine the percent cloud cover. Code provided by coauthor Hailey Goodman.

```
% Sun disc test:
clc;
clear;

area = 3.14*460.005^2;

imagefiles = dir('*.jpg');
%to give number of images found
nfiles = length(imagefiles);

for ii = 1:nfiles
    currentfilename = imagefiles(ii).name;
    currentimage = imread(currentfilename);
    images{ii} = currentimage;

    %Can be removed: but displays change in sun location over the time
    %period
    %imshow(currentimage,[]);

    %apply image segmentation
    BW = segmentImage(currentimage);
    %apply RGB color masking for sun
    BW1 = createMask(currentimage);
    %apply image region analysis
    sun = filterRegions(BW1);
%   disp(sun);

    %Test sun foot print for appropriate threshold
    if sun <= 0.3 && sun >= 0
        fprintf('Your sky is overcast\n');
        %now that we know the sky is overcast we can test for cloud layers:
        %Apply RGB color masking for bottom layer
        BWA = findbottomlayer(currentimage);
        %apply image region analysis
        bot = filterRegions(BWA);
        % present bottom layer percent
        disp(bot);
        %Apply RGB color masking for top layer
        BWB = findtoplayer(currentimage);
        %apply image region analysis
        top = filterRegions(BWB);
        % present top layer percent
        disp(top)
        %total CC
        cloudcover = top + bot;
        %Remaining space in WSI circle
        blue = 100 - cloudcover;
        disp(cloudcover);

    elseif sun >= 0.33 && sun <= 0.55
        fprintf('Your sky is clear\n');
        %Clear: does not need to test for specific cloud layers
        fprintf('There is no cloud cover to report\n');
        bot = 0;
        top = 0;
        blue = 100;
    else
        fprintf('Your sky is partly cloudy\n');
        %Partly cloudy: test for cloud layers using specifc thresholds
        %apply image segmentation
        BW = segmentImage(currentimage);
        %apply RGB color masking for sun
        PC = partlycloudyMask(currentimage);
        %apply image region analysis
        cloudcover = filterRegions(PC);
        top = 0;
        bot = 0;
        blue = 100-cloudcover;
        disp(cloudcover)
    end

end
```

Appendix G. Image Analyses Tools: Medical Applications

Image processing is used in a wide variety of applications, ranging from professional photography to digital signal processing. One of the fields in which the enhancement of images/photographs is a critical tool is medicine/health care. Often, medical imaging techniques, such as magnetic resonance imaging (MRI), radiography, and endoscopy, result in products that depend heavily on accurate and detailed representations of their subject matter. Life and recovery decisions can stem from details observed on specialized images. Many of the alternative tools mentioned in this report are also used to improve visualization and image quality for the medical community. Some examples are as follows:

- Fang et al.[1] discussed the use of image sharpening and histogram equalization to enrich texture details such as blood vessels.
- Sahnoun et al.[2] described the use of gamma correction to enhance visualization of damage or scarring of myelin sheaths, which is useful in quantifying and extracting lesions for multiple sclerosis diagnostic procedures.
- Finally, MRI data have been improved with morphological region operations. This tool helps to extract and classify brain tumors from image clusters (Zulkoffli and Shariff[3]).

[1] Fang S, Xu C, Feng B, Zhu Y. Color endoscopic image enhancement technology based on nonlinear unsharp mask and CLAHE. 2021 IEEE 6th International Conference on Signal and Image Processing (ICSIP); 2021; Nanjing, China. p. 234–239. doi.org/10.1109/icsip52628.2021.9688796.
[2] Sahnoun M, Kallel F, Dammak M, Mhiri C, Ben Mahfoudh K, Ben Hamida A. A comparative study of MRI contrast enhancement techniques based on traditional gamma correction and adaptive gamma correction: Case of multiple sclerosis pathology. 2018 4th International Conference on Advanced Technologies for Signal and Image Processing (ATSIP); 2018; Sousse, Tunisia. p. 1–7. doi.org/10.1109/atsip.2018.8364467.
[3] Zulkoffli Z, Shariff T A. Detection of brain tumor and extraction of features in MRI images using k-means clustering and morphological operations. 2019 IEEE International Conference on Automatic Control and Intelligent Systems (I2CACIS); 2019; Selangor, Malaysia. p. 1–5. doi.org/10.1109/i2cacis.2019.8825094.

List of Symbols, Abbreviations, and Acronyms

3-D	three-dimensional
AGL	above-ground level
AIHPA	Atmospheric Intelligence for Hybrid Power Advancements
AMS	American Meteorological Society
ARL	Army Research Laboratory
CRT	cathode ray tube
CLR	Clear
CLAHE	Contrast Limited Adaptive Histogram Equalization
DEVCOM	US Army Combat Capabilities Development Command
EMS	energy management system
IRC	image resolution compression
IDC	image detail compression
JPEG	Joint Photographic Experts Group (a.k.a. JPG)
LCD	Liquid-Crystal Display
LED	light-emitting diode
LiDAR	Light Detection and Ranging
LT	local time
MDT	Mountain Daylight Time
MRI	magnetic resonance imaging
MST	Mountain Standard Time
OVC	Overcast
PC	Partly Cloudy
PNG	Portable Network Graphics
PSNR	peak signal-to-noise ratio
PV	photovoltaic
QL	quality levels

RGB	red, green, blue
ROI	region of interest
SR	solar radiation
WSI	Whole Sky Imager (a.k.a. simulated Whole Sky Imager)

Distribution List

1 (PDF) DEFENSE TECHNICAL INFORMATION CTR
DTIC OCA

1 (PDF) DEVCOM ARL
FCDD RLB CI
TECH LIB

1 (PDF) ATEC
M WALTER

3 (PDF) INTERNS
S BERGEN
H GOODMAN
B WANG

1 (PDF) MTU
G PARKER

1 (PDF) C5ISR
M BAILEY

1 (PDF) GVSC
D RIZZO

11 (PDF) (5 HC) DEVCOM ARL
FCDD RLA I
T JAMESON
FCDD RLA ID
G VAUCHER (5 HC/1 PDF)
C HOCUT
R BRICE
R RANDALL
M S D'ARCY
J RABY
FCDD RLA G
M BERMAN
FCDD RLA GB
B GEIL
R JANE
FCDD RLA NA
M LEE